Optimal tuned mass-damper-inerter (TMDI) design in wind-excited tall buildings for occupants' comfort serviceability performance and energy harvesting

Francesco Petrini[1], Agathoklis Giaralis[2], Zixiao Wang[2]

[1] School of Civil and Industrial Engineering, Sapienza, University of Rome, Italy
[2] Department of Civil Engineering, City, University of London, UK

Abstract

The tuned mass-damper-inerter (TMDI) couples the classical tuned mass-damper (TMD), with an inerter device developing a resisting force proportional to the relative acceleration of its ends by the "inertance" constant. Previous works demonstrated that the inclusion of the TMDI leads to more efficient broadband vibration control for a range of different structures under different actions. This paper proposes a novel optimal TMDI design formulation to address occupants' comfort in wind-excited slender tall buildings susceptible to vortex shedding (VS) effects and to explore optimal TMDI's potential for transforming part of the wind-induced kinetic energy to usable electricity in tall buildings. Attention is focused on investigating benefits of TMDIs with different inertial properties (i.e., secondary mass/weight and inertance) configured in different topologies defined by the number of floors spanned by the inerter device to connect the secondary mass to the building structure. Optimally designed TMDIs for a wide range of inertial properties and three different topologies are obtained through numerical solution of the underlying optimization problem for a benchmark 305.9m tall building with more than 6 height-to-width ratio subjected to experimentally calibrated spatially-correlated across-wind force field accounting for VS effects. Performance-based design (PBD) graphs on the TMDI inertial (mass-inertance) plane are furnished demonstrating that any fixed structural performance level in terms of occupants' comfort (i.e., peak top floor acceleration) can be achieved through lightweight TMDIs if compared with classical TMDs as long as sufficient inertance is provided. Further, TMDI robustness to host structure properties and to reference wind velocity is shown to increase by increasing inertance or by spanning more floors in connecting the secondary mass with the host structure by the inerter. Lastly, it is found that increased available energy for harvesting in wind excited tall buildings is achieved by incorporating electromagnetic motors in TMDIs with varying damping property, while concurrent reduced floor acceleration and increased available energy for harvesting is accomplished by TMDI topologies with inerters spanning more floors.

Keywords: tuned mass damper inerter; vortex shedding; tall buildings; energy harvesting; optimal design

1. Introduction

The advent of new high strength materials and stiff lightweight structural components enabled designing and construction of increasingly slender tall buildings with height-to-width aspect ratios of 5 or more. These structures achieve efficient land utilization in congested modern city centers while reducing construction cost through reduced requirements for material usage, on-site transportation, and deep/heavy foundations among other advantages [1,2]. However, slender tall buildings with rectangular floor plan offering optimal land utilization and inner space architectural organization are prone to excessive oscillations in the across-wind direction (i.e., within the normal plane to the wind direction) due to vortex shedding (VS) effects generated around their corner edges [3-5]. These oscillations may generate floor accelerations trespassing occupants' comfort thresholds under moderate wind action (i.e., at the serviceability limit state) leading to loss of

functionality and to downtime and, thus, incurring significant losses to the users and the owners [6-11]. Increasing the lateral stiffness of tall buildings susceptible to VS induced vibrations does not improve in general serviceability limit state performance associated with peak floor accelerations [1,5]. Therefore, supplemental damping devices for motion control are often provided to slender tall buildings with rectangular footprint and appropriately designed to meet occupants' comfort requirements prescribed by building codes and guidelines within a performance-based wind engineering framework [12-13].

In this context, tuned mass-dampers (TMDs), among other devices and configurations for supplemental damping, have been widely used over the past three decades for vibration mitigation in wind-excited tall buildings [14-16]. In its simplest form, the linear passive TMD comprises an oscillating (secondary) mass attached towards the top of the building via linear stiffeners, or hangers in case of pendulum-like TMD implementations, and viscous dampers. The effectiveness of the TMD relies on "tuning" its stiffness and damping properties to the host building structure fundamental (dominant) mode of vibration for fixed attached mass, such that significant kinetic energy is transferred from the wind-excited building to the TMD secondary mass and eventually dissipated through the dampers. Apart from its use for vibration suppression, the potential of TMDs to harvest energy from wind-induced oscillations in tall buildings has been recently explored by the research community [17,18]. This consideration relies on the ability of TMDs to achieve simultaneous vibration suppression and energy generation by employing electromagnetic motors (EMs) coupled with energy harvesting/storage circuitry to replace viscous dampers in connecting the TMD mass to the host structure [18-21]. In this manner, part of the kinetic energy of the host structure is transformed into usable electric energy instead of being "lost" at the dampers in the form of heat. The thus generated energy can be stored to batteries for later use such as powering wireless sensors for structural health monitoring [20,22] or for controlling inner climate control in modern building structures [23].

Still, linear passive TMDs suffer some major drawbacks in suppressing VS induced lateral oscillations in tall buildings as identified below.

(I) TMDs may be "detuned" over time due to either unforeseen nonlinear behaviour of the TMD and/or of the host building structure, or due to changes to the dynamic properties during the service life of the host structure. Detuning affects significantly TMD vibration suppression performance which is

inherently narrow-band affecting frequencies close to the targeted dominant/fundamental natural frequency of the host structure.

(II) The effectiveness and applicability of TMDs depend heavily on the attached mass: the larger the attached mass the better vibration suppression and robustness to detuning is achieved. However, attached mass can rarely exceed 0.5% to 1% of the total building mass in tall buildings as it becomes overly expensive to accommodate its weight and volume due to structural and architectural limitations, respectively.

(III) There appears to be a trade-off between vibration suppression and energy harvesting potential in coupling TMDs with EMs for energy generation. Whilst this trade-off may not be severe for dynamic energy harvesters under broadband/white noise excitation [24], it becomes an issue for narrow-band excitations with a dominant frequency [21], as in the case of VS induced forces in the across-wind direction.

Recently, Giaralis and Petrini [25] explored the potential of incorporating an ideal inerter device to wind-excited TMD-equipped tall buildings subject to VS effects, to enhance TMD vibration suppression effectiveness. Note that the ideal inerter, rigorously defined by Smith [26], is a two-terminal mechanical element/device having negligible mass/weight and resisting relative acceleration between its terminals through a constant termed inertance and measured in (kg) units. Consequently, an inerter with one terminal/end fixed acts as a weightless mass/inertial amplifier with gain equal to the inertance [26]. This attribute of the inerter was exploited in the so-called tuned mass-damper-inerter (TMDI) configuration in [27,28], connecting the TMD mass via an inerter to a different floor from the one that the TMD is attached to, to enhance TMD vibration suppression performance in seismically excited multi-storey buildings. In [25] it was shown numerically that the TMDI achieves appreciably larger peak top floor acceleration reductions compared to the TMD in a 74-floor benchmark tall building exposed to wind-excitation accounting for VS effect. This was demonstrated through a parametric study considering non-optimal TMDI stiffness and damping coefficients for fixed attached mass and increasing inertance. This improved vibration suppression performance was attributed partly to the mass-amplification effect and partly to higher-modes-damping effect endowed to the TMD by the inerter (see also [29]). Moreover, Marian and Giaralis [30] showed analytically that in TMDIs incorporating energy harvesting EMs for kinetic energy dissipation due to single harmonic excitations in

single-degree-of-freedom (SDOF) host structures the trade-off between energy harvesting and vibration suppression may be leveraged through inerters with changing inertance as the one prototyped and experimentally verified by Brzeski et al [31], in conjunction with changes to the damping property regulated through the EM circuitry.

This paper builds on the works of Giaralis and Petrini [25] and Marian and Giaralis [30] to pursue the following two aims. The first is to quantify numerically attached mass reduction gains and improved robustness to detuning effects achieved by TMDIs optimally designed/tuned for occupants' comfort performance (serviceability limit state) in tall buildings subject to VS, therefore addressing TMD drawbacks (I) and (II). The second is to demonstrate that vibration suppression performance and available energy for harvesting trade-off can be leveraged in TMDI-equipped tall buildings susceptible to VS by considering energy harvesting enabled TMDIs with inerters spanning more floors and/or with varying damping and inertance properties in passive-adaptive mode, therefore addressing TMD drawback (III). The first aim is achieved by extending the work in [25] through pursuing optimally designed TMDIs with various inerter floor connectivity and inertance values. The second aim is pursued by extending the TMDI configuration for energy harvesting from harmonic base-excitation in SDOF structures proposed in [30] to the case of wind-excited tall buildings. In this respect, this paper contributes a novel optimal TMDI design formulation for peak top floor acceleration minimization which is solved numerically to quantify optimal tall building performance for occupants' comfort as a function of the connectivity and inertial TMDI properties (i.e., attached mass and inertance). It further contributes novel energy harvesting TMDI configurations optimally designed under the same performance criterion as above and demonstrates that available energy to harvest increases by considering TMDI configurations in which the inerter spans more than one floors as well as by letting damping and inertance properties to vary.

The aims of this paper are achieved by adopting a planar dynamical model of a 74-storey TMDI-equipped building with square floor plan as case-study structure excited by a well-established stochastic wind force model accounting for VS effect calibrated against wind tunnel tests [3]. Section 2 reviews details on the case-study structure and the wind load model. Next, Section 3 discusses modelling and analysis of the case-study structure equipped with TMDIs in different inerter floor connectivity. Section 4 presents the optimal TMDI design formulation and numerical solution for serviceability limit state (occupants' comfort) in wind-excited tall buildings and probes into the properties of optimal TMDI equipped case-study structure. In Section

5 the performance of optimal TMDI designs for occupants' comfort is verified and gains in secondary mass are quantified. In Section 6, TMDI robustness to detuning due to change of properties of the host case-study structure is investigated and the applicability of using inerters to upgrade performance of existing TMD-equipped tall buildings is explored. Section 7 considers energy harvesting enabled TMDI configurations optimally designed of occupants' comfort for the case-study structure and demonstrates numerically the gains in available energy for harvesting as requirements for vibration suppression are relaxed through varying TMDI inertance and damping properties. Finally, Section 8 summarizes conclusions and points to directions for future research.

2. Modelling of case-study building structure and wind force excitation

2.1 Benchmark building description and finite element modelling

A slender 74-storey steel frame building with height-to-width aspect ratio of more than 6 is taken as a case-study structure throughout this work. The building has rectangular 50x50 (m) footprint and is 305.9m high: typical floor height is 4m, while ground and last floor height is 13m and 4.9m, respectively. The adopted structure is sensitive to VS induced vibrations compromising occupants' comfort and has been previously considered as benchmark for the development of a performance-based wind engineering framework [13,32]. The lateral load bearing system of the case-study structure is double-symmetric along two horizontal perpendicular principal axes. It comprises an inner and an outer spatial steel frame having 12 and 28 columns, respectively. The two frames are connected by three steel truss outriggers spaced approximately 100m apart. All columns have hollow square sections, with varying dimensions and thickness along the building height ranging between 1.20mx1.20m to 0.50mx0.50m, and 0.06m to 0.025m, respectively. Beams are of various standard double-T steel section profiles while outriggers consist of double-T horizontal and hollow-square diagonal members. A finite element (FE) model of the considered structural system is shown in Fig. 1. The FE model comprises 7592 linear Euler-Bernoulli beam elements with all beam-to-column connections taken as rigid. Horizontal rigid diaphragm constraints are imposed at the height of each floor to account for the effect of the slabs in the model. The total mass of the structure accounting for dead and live loads is 92830tons and is uniformly distributed at each floor level except for the last floor to which half of the typical floor mass is assigned.

Due to the presence of VS, the direction of the wind field which maximizes lateral wind-induced vibrations (floor accelerations) in the across-wind direction coincides with any of the two principal axes of the adopted structure [13]. Therefore, only the uncoupled purely translational modes of vibration of the FE model along a principal building axis are required for the assessment of structural performance in terms of occupants' comfort serviceability limit state. For illustration, the first six translational mode shapes along a horizontal principal building axis are plotted in Fig.1 tracing nodal displacements of the master node of each floor. They are obtained from standard linear modal analysis upon constraining all rotational degrees of freedom (DOFs) about the gravitational axis and all translational DOFs along the perpendicular horizontal principal axis of the building. The first three natural frequencies of these modes and the corresponding modal participating mass ratios in parentheses are 0.185Hz (0.6233), 0.563Hz (0.1900), and 1.052Hz (0.0745).

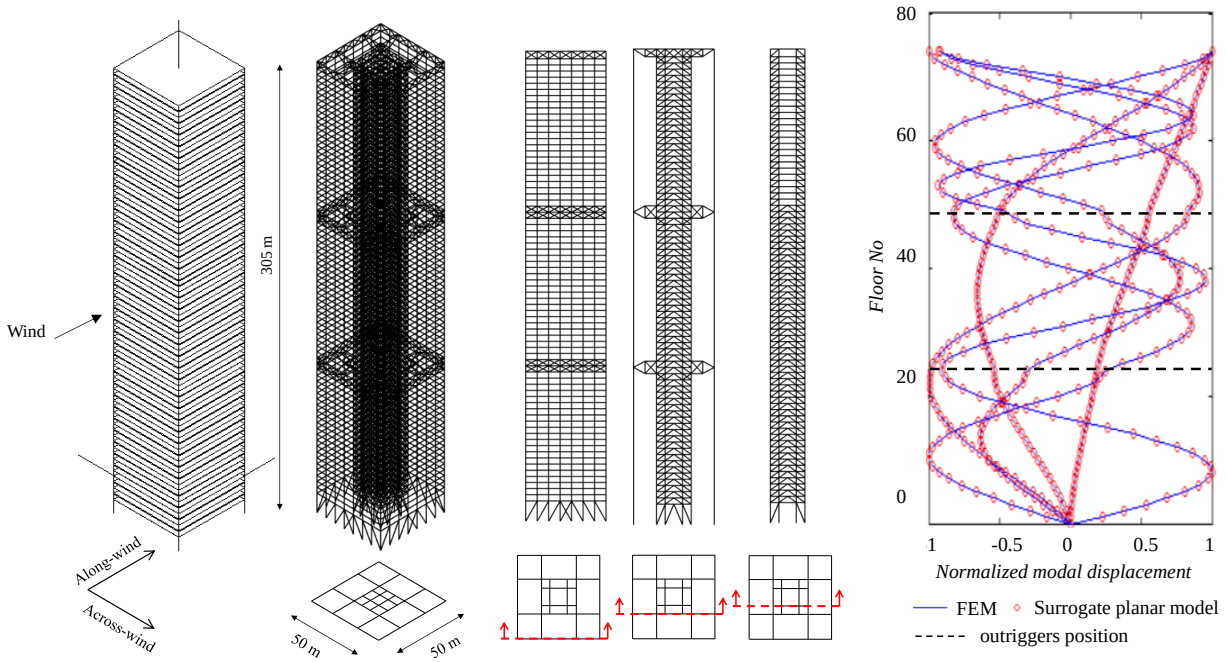

Figure 1. Detailed FE model of the adopted benchmark case-study tall building structure and in-plan lateral translational mode shapes.

2.2 Surrogate planar frame model

The fact that the critical response of the adopted case-study building to wind excitation lies along any one structural principal axis motivates the consideration of a surrogate planar (two-dimensional) dynamical model capturing faithfully the in-plane lateral vibrational behavior along a principal axis of the high-fidelity three-dimensional FE model of Fig.1. The considered model has N=74 DOFs corresponding to the lateral translational displacements of the 74 rigid diaphragms, one at each floor, along a principal horizontal axis of

symmetry of the case-study building. It, therefore, can be viewed as a 74-storey planar frame supporting, in later sections, the physical tractability of different TMDI topologies involving different floor connectivity.

Mathematically, the adopted planar model is defined in terms of mass, $\mathbf{M_s} \in \mathbb{R}^{74\times74}$, damping, $\mathbf{C_s} \in \mathbb{R}^{74\times74}$, and stiffness, $\mathbf{K_s} \in \mathbb{R}^{74\times74}$ matrices such that: (i) its undamped 74 modes of vibration match the 74 lateral uncoupled translational modes of the FE model of the case-study structure in Fig. 1, and (ii) it attains frequency-dependent damping properties specified based on recorded measurements from real-life tall buildings reported in the literature [33]. Notably, the definition of the planar frame model through $\mathbf{M_s}$, $\mathbf{C_s}$, and $\mathbf{K_s}$ matrices enables, later, the incorporation of the TMDI through straightforward matrix manipulations rather than modifications to the detailed FE model.

Following [25], condition (i) is met by first defining a diagonal mass matrix $\mathbf{M_s}$ with diagonal elements equal to the floor masses assumed by the FE model. That is, $M_s(k,k)$= 1263ton (k=1,2,…,73) and $M_s(74,74)$= 631ton. Next, a full stiffness matrix $\mathbf{K_s}$ is obtained by satisfying the modal analysis equations

$$\left[\mathbf{K_s} - \omega^2_{(\mathrm{FE})_j}\mathbf{M_s}\right]\boldsymbol{\varphi}_{(\mathrm{FE})_j} = 0 \quad ; \quad j = 1,2,...,74, \tag{1}$$

where $\boldsymbol{\varphi}_{(\mathrm{FE})_j} \in \mathbb{R}^{74\times1}$ is the j-th uncoupled translational mode shape along a principal building axis obtained from the detailed FE model as previously discussed and $\omega_{(\mathrm{FE})j}$ is the corresponding natural frequency. Excellent quality of mode shape matching is achieved as illustrated in the rightmost panel of Fig. 1 in which the first six normalized mode shapes obtained from the FE model, $\boldsymbol{\varphi}_{(\mathrm{FE})j}$ (j=1,2,…,6) and from the planar frame model, $\boldsymbol{\varphi}_j$ (j=1,2,…,6), are superposed plotted as continuous lines and circle-shaped dots, respectively. Further, a full damping matrix is obtained by the expression

$$\mathbf{C_s} = \left(\boldsymbol{\Phi}^T\right)^{-1}\mathbf{C}_{\mathrm{mod}}\left(\boldsymbol{\Phi}\right)^{-1} \tag{2}$$

where $\boldsymbol{\Phi} \in \mathbb{R}^{74\times74}$ is the modal matrix collecting all 74 $\boldsymbol{\varphi}_j$ mode shapes, the superscript "-1" denotes matrix inversion, and $\mathbf{C_{mod}} \in \mathbb{R}^{74\times74}$ is a diagonal matrix defined as

$$\mathbf{C_{mod}}\left(j,j\right) = 2\omega_j\xi_j\left(\boldsymbol{\varphi}_j{}^T\mathbf{M_s}\boldsymbol{\varphi}_j\right) \quad ; \quad j = 1,2,...,74 \tag{3}$$

In the last equation, ω_j and ξ_j are the j-th natural frequency and modal damping ratio, respectively, of the planar frame model. In meeting condition (ii) above, damping ratios are taken equal to: ξ_j=2%, for j= 1,2,3; ξ_j= 4%

for j= 4,5,6; ξ_j= 6% for j= 7,8,9,10; ξ_j=9% for j= 11,12,…,20; ξ_j=12% for j= 21,22,…,40; ξ_j=15% for j=41,42,…,60; and ξ_j=18% for j=61,62,…,74. Damping ratios in the frequency range of 0-7Hz are specified to match experimentally identified damping ratios from full-scale field measurements in tall steel framed buildings reported in [33] and references therein. For frequencies above this range, the value of modal damping ratios increases gradually to account for the anticipated greater participation of non-structural components to the inherent damping of the structure for oscillations dominated by the higher vibration modes [25].

2.3 Wind force excitation model

The input wind action to the 74-storey planar frame model derived in the previous section is herein represented by the stochastic across-wind force model developed in [3] for tall buildings with rectangular footprint. The adopted model is based on experimental data from a comprehensive wind tunnel testing campaign and accounts for both the turbulence and the VS components of the across wind force, the latter being critical for occupants' comfort in the case-study building [13]. It is defined by a zero-mean Gaussian ergodic spatially correlated random field expressed in the domain of circular frequencies ω analytically through a power spectral density (PSD) matrix. Upon spatial discretization of the wind force random field at each floor slab of the case-study 74-storey building, a PSD $\mathbf{S}_{\mathbf{FF}}^{\mathbf{74}} \in \mathbb{R}^{74\times 74}$ wind force matrix is specified. For the case-study building with total height 305.9m and square footprint the diagonal elements of the PSD wind force matrix, are given as [3]

$$S_{FF}^{74}[k,k]=\frac{\sigma_k^2}{\omega}\left[\frac{0.1032\left(\omega/\omega_k\right)^2}{\left(1-\left(\omega/\omega_k\right)^2\right)^2+0.031\left(\omega/\omega_k\right)^2}+\frac{0.1278\left(\omega/\omega_k\right)^3}{\left(1-\left(\omega/\omega_k\right)^2\right)^2+2\left(\omega/\omega_k\right)^2}\right], k=1,2,...,74 \tag{4}$$

which specify the PSD of the wind force acting at the k-th floor slab located at height z_k from the ground. In the previous expression, σ_k is the root mean square (RMS) of the across wind force at the k-th floor slab and ω_k is the frequency of VS at z_k height. The RMS of the across wind force is herein computed as

$$\sigma_k=\frac{1}{2}\rho V_{\mathrm{m}}^2(z_k)\bar{C}_{\mathrm{L}}B\Delta z_k\,, \tag{5}$$

where ρ is the air mass density taken equal to 1.25kg/m^3; $\bar{C}_{\mathrm{L}}$ is the mean RMS lift coefficient which is equal to 0.404 for square footprint buildings according to [3]; B= 50m is the width of the building in the across-wind

direction; Δz_k is the tributary height of the *k*-th floor taken as half the storey height above floor *k* plus half the storey height below floor *k*; and $V_m(z_k)$ is the mean wind velocity at z_k height. The latter can be determined through the power law expression [34]

$$V_m(z) = V_{ref}\left(\frac{z}{H_{ref}}\right)^a, \tag{6}$$

where V_{ref} is a reference gradient wind velocity controlling the intensity of the wind action at height H_{ref} above the ground, and α is a dimensionless parameter dependent on the site terrain roughness. For the purposes of this paper, V_{ref} is assumed to be the design wind speed for the case-study building with one year return period commonly specified in building codes to check for occupants' comfort criteria [35]. Moreover, the α parameter is taken equal to 0.35 which is consistent with large cities terrain type [34], while H_{ref} is pinned to 810m assumed as a characteristic height of the atmospheric boundary layer in congested urban environments. Further, the VS frequency in Eq.(4) is determined by

$$\omega_k = \frac{2\pi S_t V_m(z_k)}{B}, \tag{7}$$

in which S_t is the Strouhal number taken equal to 0.084 as experimentally determined in [3] for square footprint tall buildings.

For illustration, the PSDs of wind force acting at four different floor slab heights are plotted in Fig. 2 for V_{ref}= 30m/s. It is seen that the dominant VS frequency increases with floor height as can be inferred by Eqs. (6) and (7). The same happens for the wind force amplitude except from the first and last floors whose tributary heights are different from the rest of the building floors, i.e., 8.5m and 2.45m, respectively as opposed to 4m for typical floor.

Lastly, the off-diagonal terms of the $\mathbf{S}_{\mathbf{FF}}^{\mathbf{74}}$ PSD matrix modelling the spatial correlation of wind forces acting at floor slabs *k* and *l* are given as [3]

$$S_{FF}^{74}[k,l] = \exp\left[-\left(\frac{z_k - z_l}{278}\right)^2\right]\sqrt{S_k(\omega)S_l(\omega)}, \tag{8}$$

for the case-study building.

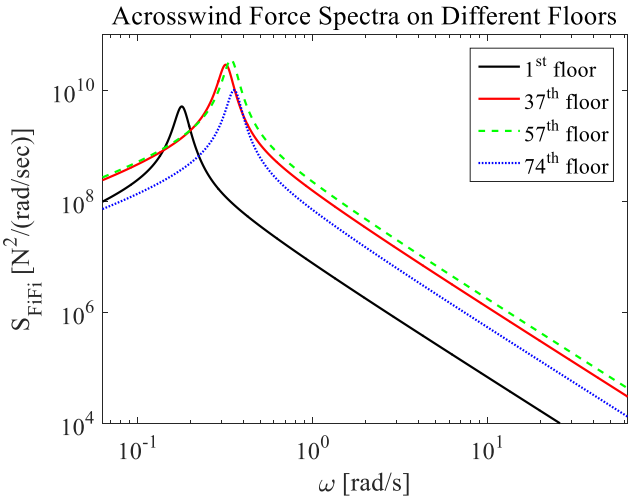

Figure 2. Power spectral density functions (PSDs) of cross-wind forces acting at different floor levels of the case-study structure.

3 TMDI-equipped tall building modelling and structural analysis for across-wind excitation

3.1 Incorporation of TMDI to the planar frame model of case-study structure in different topologies

The tuned mass damper inerter (TMDI) is a linear passive dynamic vibration absorber introduced in [27-28] for supressing the lateral motion of seismically excited multi-storey building structures amenable to modelling as planar MDOF systems with mass properties lumped at each floor. Following [25], a TMDI is herein considered to mitigate wind-induced accelerations in the across-wind direction of the benchmark structure. The modelling of the TMDI and its incorporation to the adopted structure is graphically shown in Fig. 3 depicting the 74-DOF surrogate model derived in section 2.2 as a planar 74-storey frame-like building with lumped floor masses $m_k = M_s(k,k)$; k=1,2,…,74. The TMDI consists of a conventional TMD comprising a secondary m_{TMDI} mass attached to the top floor via a stiffener, modelled as a linear spring with k_{TMDI} stiffness, in parallel with a linear viscous damper, modelled as a dashpot with damping coefficient c_{TMDI}, and an inerter device, highlighted in red in Fig. 3, connecting the secondary mass to p floors below the top floor. The inerter device is modelled through an ideal massless/weightless mechanical element resisting the relative acceleration developing at its two ends/terminals through the inertance coefficient b [26]. In this regard, the inerter element force reads as

$$F_b = b\left(\ddot{x}_{TMDI} - \ddot{x}_{74-p}\right), \tag{9}$$

where x_{TMDI} is the lateral displacement of the secondary mass, x_{74-p} is the lateral displacement of the floor which the inerter connects the secondary mass to and a dot over a symbol signifies differentiation with respect to time. Therefore, in the TMDI configuration the inerter exerts an additional, compared to the conventional TMD, control force, F_b, to the host structure whose amplitude depends on the relative acceleration of the inerter terminals and on the inertance b. In this regard, the potentially improved vibration suppression capability of the TMDI compared to the TMD depends on the inerter connectivity (i.e., number of floors p spanned by the inerter as shown in Fig. 3), hereafter denoted as "-p" TMDI topology, as well as on the inertance b. The influence of both the above TMDI properties are examined in the numerical part of the paper through optimal TMDI tuning and structural performance assessment for different TMDI topologies and inertance values.

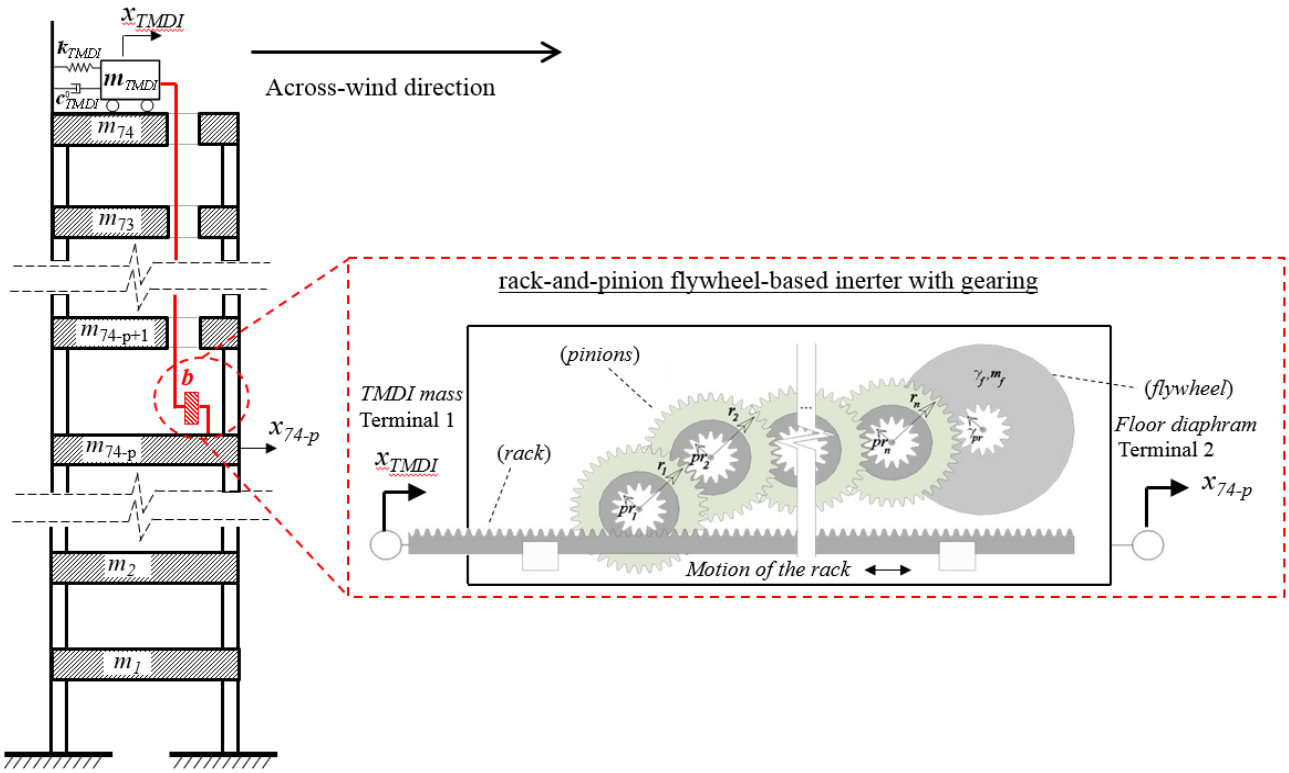

Figure 3. TMDI equipped lumped-mass surrogate planar frame model of the wind-excited case-study building with "-p" topology and typical rack-and-pinion flywheel inerter device with n gears.

With regards to TMDI topology, the cases p=1, 2, and 3 are examined later in this work taken to be mostly appealing to potential practical implementations involving a pendulum-like TMDI accommodated within a central atrium spanning up to three highest building floors in a similar manner to existing pendulum TMD applications (e.g., Taipei 101 building). Further discussion on practical considerations of TMDI topologies with p>1 can be found in [25,36]. Turning the attention to the inertance property, b, it is important to note it is readily scalable and independent of the physical mass/weight of the inerter device in a similar

manner to the scalability of the damping coefficient c_{TMDI} of the TMDI viscous damper. Indeed, supplemental damping devices for seismic protection of building structures incorporating inerters with several hundred thousand tons of inertance have been prototyped and experimentally verified in recent years [37,38]. To shed further light on this issue, consider a commonly used inerter device embodiment employing a rack-and-pinion mechanism to transform the translational motion into rotational motion of a flywheel (i.e., a solid spinning disk) through a gearbox shown in Fig. 3. It can be readily shown the inertance of this device is given as [26]

$$b = m_f \frac{\gamma_f^2}{\gamma_{pr}^2}\left(\prod_{q=1}^{n}\frac{r_q^2}{pr_q^2}\right) \tag{10}$$

where m_f and γ_f are the mass and radius of the gyration of the flywheel, respectively, γ_{pf} is the radius of gyration of the flywheel pinion, $r_q/(pr_q)$ is the gearing ratio of the q-th stage/gear of the gearbox with n stages. Clearly, the inertance can be scaled by orders of magnitude through changing the gearing ratios and/or the number of the gears with immaterial change to the mass/weight of the device. Along these lines, Brzeski et al. [31] demonstrated experimentally the feasibility of inerter devices with continuously varying transmission gearbox, rather than stepped gearing changes, leading to inerters that may achieve any desired inertance value, within the gearbox effective range of transmission.

Mathematically, the mass, **M**, the damping, **C**, and the stiffness, **K**, matrices of the surrogate building model equipped with a TMDI configured in "-p topology" are concisely written as [25]

$$\begin{aligned}
\mathbf{M} &= \mathbf{M}_\mathbf{s}^+ + (m_{TMDI}+b)\mathbf{1}_{75}\mathbf{1}_{75}^T + b\mathbf{1}_{74\text{-}\mathbf{p}}\mathbf{1}_{74\text{-}\mathbf{p}}^T - b\left(\mathbf{1}_{75}\mathbf{1}_{74\text{-}\mathbf{p}}^T + \mathbf{1}_{74\text{-}\mathbf{p}}\mathbf{1}_{75}^T\right)\\
\mathbf{C} &= \mathbf{C}_\mathbf{s}^+ + c_{TMDI}\left(\mathbf{1}_{75}\mathbf{1}_{75}^T + \mathbf{1}_{74}\mathbf{1}_{74}^T - \mathbf{1}_{75}\mathbf{1}_{74}^T - \mathbf{1}_{74}\mathbf{1}_{75}^T\right)\\
\mathbf{K} &= \mathbf{K}_\mathbf{s}^+ + k_{TMDI}\left(\mathbf{1}_{75}\mathbf{1}_{75}^T + \mathbf{1}_{74}\mathbf{1}_{74}^T - \mathbf{1}_{75}\mathbf{1}_{74}^T - \mathbf{1}_{74}\mathbf{1}_{75}^T\right)
\end{aligned} \tag{11}$$

In the above expressions, $\mathbf{M}_\mathbf{s}^+ \in \mathbb{R}^{75\times75}$, $\mathbf{C}_\mathbf{s}^+ \in \mathbb{R}^{75\times75}$, and $\mathbf{K}_\mathbf{s}^+ \in \mathbb{R}^{75\times75}$ are the mass, $\mathbf{M}_\mathbf{s} \in \mathbb{R}^{74\times74}$, the damping, $\mathbf{C}_\mathbf{s} \in \mathbb{R}^{74\times74}$, and the stiffness, $\mathbf{K}_\mathbf{s} \in \mathbb{R}^{75\times75}$, matrices of the surrogate planar frame model defined in section 2.2, respectively, augmented by one last (bottom) row with zero entries and by one last (rightmost) column with zero entries. Further, the vector $\mathbf{1}_\mathbf{u} \in \mathbb{R}^{75\times1}$ has zero element except from the u-th entry which is equal to one, and the superscript "*T*" denotes matrix transposition. Note that the inclusion of the inerter influences only the mass matrix **M** of the controlled surrogate building model in Eq.(11), that is, matrices **C** and **K** are the

same for the TMD and for the TMDI. More importantly, note that for *b=0* (no inerter), Eq.(11) represents the surrogate building model with a conventional TMD attached to its top, 74-th, floor, which is the most widely considered TMD topology for vibration suppression in wind-excited tall buildings (see e.g. [15,16]). Therefore, in the ensuing numerical work, the TMD is treated as a special case of the TMDI by setting *b*=0.

3.2 Frequency-domain across-wind response analysis of TMDI-equipped surrogate model

Optimal TMDI design/tuning for the adopted case-study building discussed in the next section, requires computationally efficient determination of peak response of the TMDI-equipped surrogate model defined through the **M**, **C**, and **K** matrices in Eq.(11) subject to the wind force excitation model discussed in section 2.3. This is herein facilitated through structural analysis in frequency domain. Specifically, the response displacement, velocity, and acceleration PSD matrices of the TMDI-equipped surrogate model due to the $\mathbf{S}_{\mathbf{FF}}^{\mathbf{74}}$ wind force PSD matrix defined in section 2.3 are obtained using the frequency domain input-output relationships of random vibrations [39]

$$\mathbf{S}_{\mathbf{xx}}(\omega)=\mathbf{B}(\omega)^{*}\mathbf{S}_{\mathbf{FF}}(\omega)\mathbf{B}(\omega),\quad \mathbf{S}_{\dot{\mathbf{x}}\dot{\mathbf{x}}}(\omega)=\omega^{2}\mathbf{S}_{\mathbf{xx}}(\omega),\ \text{and}\quad \mathbf{S}_{\ddot{\mathbf{x}}\ddot{\mathbf{x}}}(\omega)=\omega^{4}\mathbf{S}_{\mathbf{xx}}(\omega), \tag{12}$$

respectively. In Eq. (12), $\mathbf{S}_{\mathbf{FF}}$ is the PSD wind force matrix $\mathbf{S}_{\mathbf{FF}}^{\mathbf{74}}$ defined in section 2.3, augmented by a zero row and a zero column corresponding to the DOF of the TMDI which is not subjected to any wind load (internally housed). Further, the "*" superscript denotes complex matrix conjugation, and the transfer matrix **B** is given as

$$\mathbf{B}(\omega)=\left(\mathbf{K}-\omega^{2}\mathbf{M}+i\omega\mathbf{C}\right)^{-1} \tag{13}$$

where $i=\sqrt{-1}$.

Next, the response displacement, velocity and acceleration variances of the *k*-th floor for the TMDI-equipped surrogate model are obtained as

$$\sigma_{x_k}^{2}=\int_{0}^{\omega_{\max}} S_{x_kx_k}(\omega)\,d\omega,\quad \sigma_{\dot{x}_k}^{2}=\int_{0}^{\omega_{\max}} S_{\dot{x}_k\dot{x}_k}(\omega)\,d\omega,\ \text{and}\quad \sigma_{\ddot{x}_k}^{2}=\int_{0}^{\omega_{\max}} S_{\ddot{x}_k\ddot{x}_k}(\omega)\,d\omega \tag{14}$$

respectively. That is, by integrating the response auto-spectra populating the main diagonal elements of the response PSDs in Eq. (12), $S_{x_kx_k}(\omega)=S_{xx}[k,k]$, $S_{\dot{x}_k\dot{x}_k}(\omega)=S_{\dot{x}\dot{x}}[k,k]$, and $S_{\ddot{x}_k\ddot{x}_k}(\omega)=S_{\ddot{x}\ddot{x}}[k,k]$, up to a

maximum (cut-off) frequency, ω_{max}, above which the energy of the underlying stochastic processes is negligible. Furthermore, the variance of the relative response displacement, velocity, and acceleration between two different floors, or more generally between two different DOFs, *k* and *l* is obtained by

$$\begin{aligned}
\sigma_{x_{kl}}^2 &= \sigma_{x_k}^2 + \sigma_{x_l}^2 - 2\int_0^{\omega_{\max}} S_{x_k x_l}(\omega)\, d\omega, \\
\sigma_{\dot{x}_{kl}}^2 &= \sigma_{\dot{x}_k}^2 + \sigma_{\dot{x}_l}^2 - 2\int_0^{\omega_{\max}} S_{\dot{x}_k \dot{x}_l}(\omega)\, d\omega, \text{ and} \\
\sigma_{\ddot{x}_{kl}}^2 &= \sigma_{\ddot{x}_k}^2 + \sigma_{\ddot{x}_l}^2 - 2\int_0^{\omega_{\max}} S_{\ddot{x}_k \ddot{x}_l}(\omega)\, d\omega,
\end{aligned} \tag{15}$$

where $S_{\dot{x}_k \dot{x}_l}(\omega) = S_{\dot{x}\dot{x}}[k,l]$ and $S_{\ddot{x}_k \ddot{x}_l}(\omega) = S_{\ddot{x}\ddot{x}}[k,l]$ are the response velocity and acceleration cross-spectra corresponding to the *k* and *l* DOFs. Ultimately, the peak displacement, velocity and acceleration of the *k*-th DOF are estimated by the expressions

$$\text{peak}\{x_k\} = g\sqrt{\sigma_{x_k}^2}, \quad \text{peak}\{\dot{x}_k\} = g\sqrt{\sigma_{\dot{x}_k}^2}, \text{ and} \quad \text{peak}\{\ddot{x}_k\} = g\sqrt{\sigma_{\ddot{x}_k}^2}, \tag{16}$$

respectively, and the peak relative displacement, velocity, and acceleration between *k* and *l* DOFs, are estimated by the expressions

$$\text{peak}\{x_{kl}\} = g\sqrt{\sigma_{x_{kl}}^2}, \quad \text{peak}\{\dot{x}_{kl}\} = g\sqrt{\sigma_{\dot{x}_{kl}}^2}, \text{ and} \quad \text{peak}\{\ddot{x}_{kl}\} = g\sqrt{\sigma_{\ddot{x}_{kl}}^2}, \tag{17}$$

respectively. In the Eqs. (16) and (17), *g* is the peak factor estimated by the widely used empirical formula due to Davenport [40]

$$g = \sqrt{2ln(\eta T_{wind})} + \frac{0.577}{\sqrt{2ln(\eta T_{wind})}}, \tag{18}$$

where $\eta = 2\pi/\omega$ is the effective structural response frequency in Hz (e.g., can be taken equal to the fundamental natural frequency of the uncontrolled surrogate structural model), and T_{wind} is an assumed time duration of exposure to the wind action during which the peak response quantities in Eqs.(16) and (17) are evaluated under the common assumption of stochastic input/output processes being stationary/ergodic time-limited processes.

4. Optimal TMDI design for occupants comfort

4.1 Optimal problem formulation

To explore the full potential of TMDI for motion control in wind-excited slender tall buildings susceptible to VS, a novel optimization problem is herein formulated and solved numerically to design/tune TMDI parameters for occupants' comfort. Since the maximum wind-induced peak floor acceleration is always attained at the top floor of the case-study building [12,13], the proposed optimal TMDI design problem aims to minimize the peak top floor acceleration $\text{peak}\{\ddot{x}_{74}\}$ in Eq. (16) attained within one hour of excitation, that is taking T_{wind}=3600s in Eq. (18), under the wind force PSD matrix $\mathbf{S_{FF}}$ in Eq. (12) specified for a given design reference wind speed V_{ref} in Eq. (6). The considered optimization problem involves four dimensionless design parameters, namely the TMDI frequency and damping ratios defined as

$$\upsilon_{TMDI}=\frac{\sqrt{\dfrac{k_{TMDI}}{(m_{TMDI}+b)}}}{\omega_1} \quad \text{and} \quad \xi_{TMDI}=\frac{c_{TMDI}}{2\sqrt{(m_{TMDI}+b)k_{TMDI}}}, \tag{19}$$

respectively, where ω_1 is the first natural frequency of the case-study building, and grouped in the vector $\mathbf{x}_1$=[υ_{TMDI}, ξ_{TMDI}]$^{\text{T}}$, as well as the mass and inertance ratios defined as

$$\mu=\frac{m_{TMDI}}{M_{tot}} \quad \text{and} \quad \beta=\frac{b}{M_{tot}}, \tag{20}$$

respectively, where M_{tot} is the total building mass, grouped in the vector $\mathbf{x}_2$=[μ, β]$^{\text{T}}$. The optimization problem is solved numerically using a pattern search algorithm [41] to determine design parameters in $\mathbf{x}_1$ (primary design parameters) within a pre-specified search range [$\mathbf{x}_1^{\min}$, $\mathbf{x}_1^{\max}$] that minimize the adopted objective function (OF), $\text{peak}\{\ddot{x}_{74}\}$, given values of the parameters in $\mathbf{x}_2$ (secondary design parameters). The problem can be mathematically expressed as

$$\min_{\mathbf{x}_1}\left[\text{OF}\left(\mathbf{x}_1|\mathbf{x}_2\right)\right], \quad \text{where} \quad \text{OF}=\text{peak}\{\ddot{x}_{74}\}, \quad \text{subjected to} \quad \mathbf{x}_1^{\min}\le\mathbf{x}_1\le\mathbf{x}_1^{\max}. \tag{21}$$

Purposely, the above optimal design formulation allows for considering explicitly any desired combination of TMDI inertial properties, that is, attached mass and inertance, through the secondary design

parameters μ and β, respectively. In this manner, the special case of the TMD (β=0) can be examined and, to this effect, the bounds of υ_{TMDI} and μ values are set to [0.8,1.2] and [0.1%,1%], respectively, based on real-life TMD installations tuned to the first/fundamental mode shape of high-rise buildings. Further, ξ_{TMDI} and β are limited to maximum values of 0.8 to avoid unrealistically high viscous damping coefficients and inertance for the considered structure. In this regard, the search range used in solving Eq.(21) is taken as $\mathbf{x}_1^{\min}=[0.2\ 0.01]^{\mathrm{T}}$ and $\mathbf{x}_1^{\max}=[1.2\ 0.8]^{\mathrm{T}}$. This range was proved sufficient for the adopted structure for TMDI inertial properties spanning $0.1\% \le \mu \le 1\%$ and $0 \le \beta \le 0.8$ for practically relevant TMDI topologies p= 1,2,3 and for V_{ref} up to 50m/s.

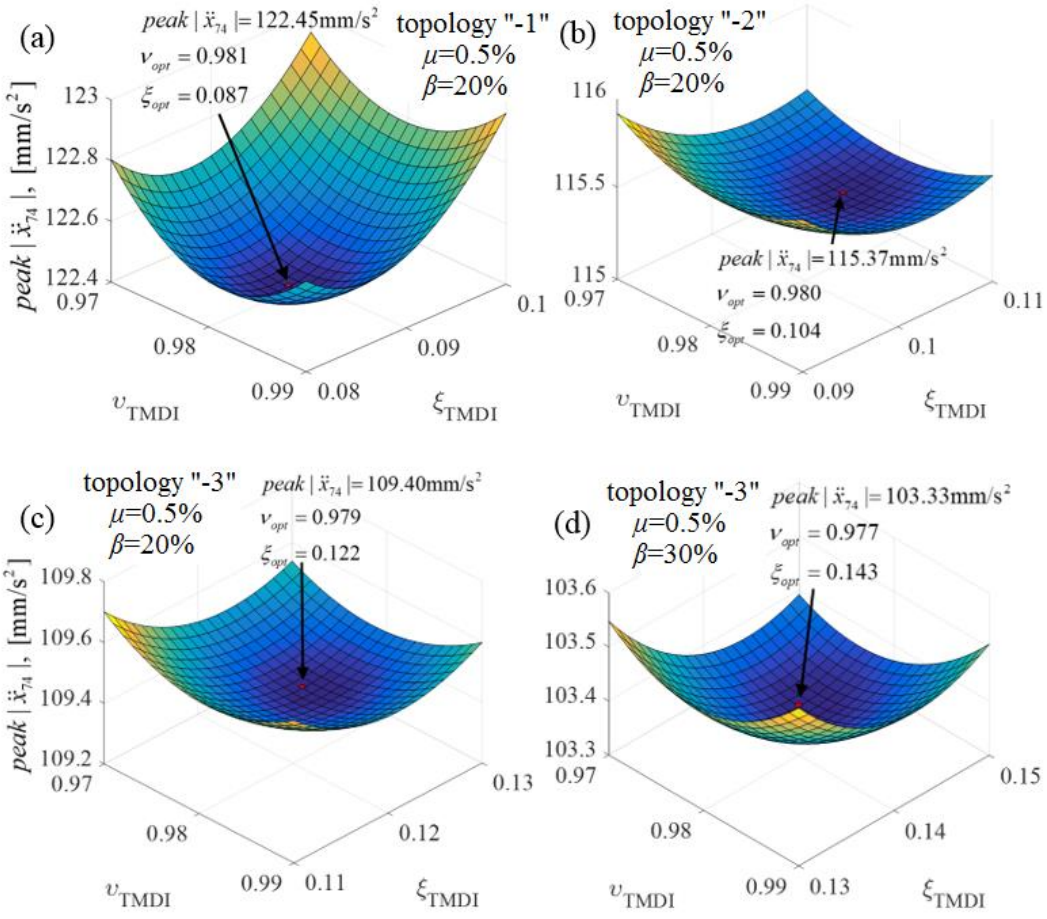

Figure 4. Objective function and design point of the optimization problem in Eq.(21) for μ=0.5%, V_{ref}=30m/s and for different TMDI topologies and inertance ratios.

4.2 Convexity and optimality of the TMDI design problem

From a computational viewpoint, strong convex behavior of the objective function OF= $\text{peak}\{\ddot{x}_{74}\}$ on the primary design variables υ_{TMDI}-ξ_{TMDI} plane is noted with a single prominent global optimal design point

being observed for all TMDI cases considered. For illustration, Figs. 4(a)-4(c) plot the $\text{peak}\{\ddot{x}_{74}\}$ as a function of the primary design variables for fixed μ=0.5%, β=20%, and V_{ref}=30m/s and for three different TMDI topologies, i.e., p=1,2,3 in Fig. 3 demonstrating that convexity of the optimization problem in Eq. (21) is maintained for all TMDI topologies herein examined. Moreover, Figs. 4(c) and 4(d) plot the $\text{peak}\{\ddot{x}_{74}\}$ response surface on the primary variables plane for fixed μ=0.5%, TMDI topology "-3", and V_{ref}=30m/s and for two different inertance ratio values illustrating that the problem in Eq.(21) is convex irrespective of the assumed inertance value.

To shed light on the nature of the motion control achieved through solving Eq.(21), Fig. 5 plots frequency response functions (FRFs) of top floor acceleration of the case-study structure equipped with TMDIs optimally designed for V_{ref}=30m/s and for various topologies and inertance ratios, β, including the limiting case of β=0 (TMD). All inertial dampers considered have the same attached mass μ=0.5%, while the FRF of the uncontrolled model is also superposed. The left column panels of Fig.5 focuses on the FRFs behaviour within a narrow frequency range around the first/fundamental natural frequency of the uncontrolled structure and the two lowest natural frequencies of the TMD(I) controlled structures. It is seen in Fig.5(a), considering TMDIs with fixed ("-3") topology and varying inertance, that the solution of the proposed optimal TMDI design formulation yields a "Den Hartog" style of optimality at least for $\beta\leq$20% in the sense that the two resonant peaks of the controlled structure attain almost equal FRF values. This type of optimality is mostly efficient for supressing narrow-band excitations characterized by a dominant frequency (see also [30]) and, therefore, relevant to problem at hand (see Figure 2). Nevertheless, as the inertance increases above 20% the right-most peak value in the FRFs becomes lower than the left-most peak value. Further, a shift of the first resonant frequency to lower frequencies is observed as inertance increases for fixed μ and topology in the FRFs of TMDI-controlled structure, while the second resonant frequency is attained at higher frequencies. Overall, the FRF value at the fundamental natural frequency of the uncontrolled structure reduces considerably with increasing inertance, however, the controlled structure attains larger FRF values compared to the uncontrolled structure at a relatively narrow band of frequencies lower than the fundamental natural frequency of the uncontrolled structure. Interestingly, all the above discussed trends in the FRFs of optimal TMDI-equipped case-study structure with increasing inertance hold true for the case of TMDI-equipped structure with fixed attached mass μ=0.5% and inertance β= 30% as the inerter spans more floors, that is, as TMDI topologies with

increasing *p* are considered shown in Fig. 5(c). The latter observation suggests that increasing the number of floors spanned by the inerter has a similar effect to the FRFs of optimal TMDI-equipped structures as the increase of the inertance for fixed TMDI topology. More importantly, the FRFs in the right column panels of Fig. 5, plotted for a wider frequency range to include the first three natural frequencies of the uncontrolled structure, demonstrate that TMDIs optimally designed through the problem formulation in Eq.(21) suppress higher modes of vibration. Notably, this is not the case for the TMD. Specifically, appreciable reductions to peak FRF values corresponding to higher vibration modes for optimal TMDI-equipped structures are achieved as the inertance increases for fixed TMDI topology, Fig. 5(b), and as the inerter device spans more floors for fixed inertance, Figs. 5(d). To this end, it is established that increasing inertance for fixed TMDI topology and secondary mass affect qualitatively the FRF of $\text{peak}\{\ddot{x}_{74}\}$ in the same manner as by increasing the number of floors spanned by the inerter in TMDIs with fixed inertance and secondary mass.

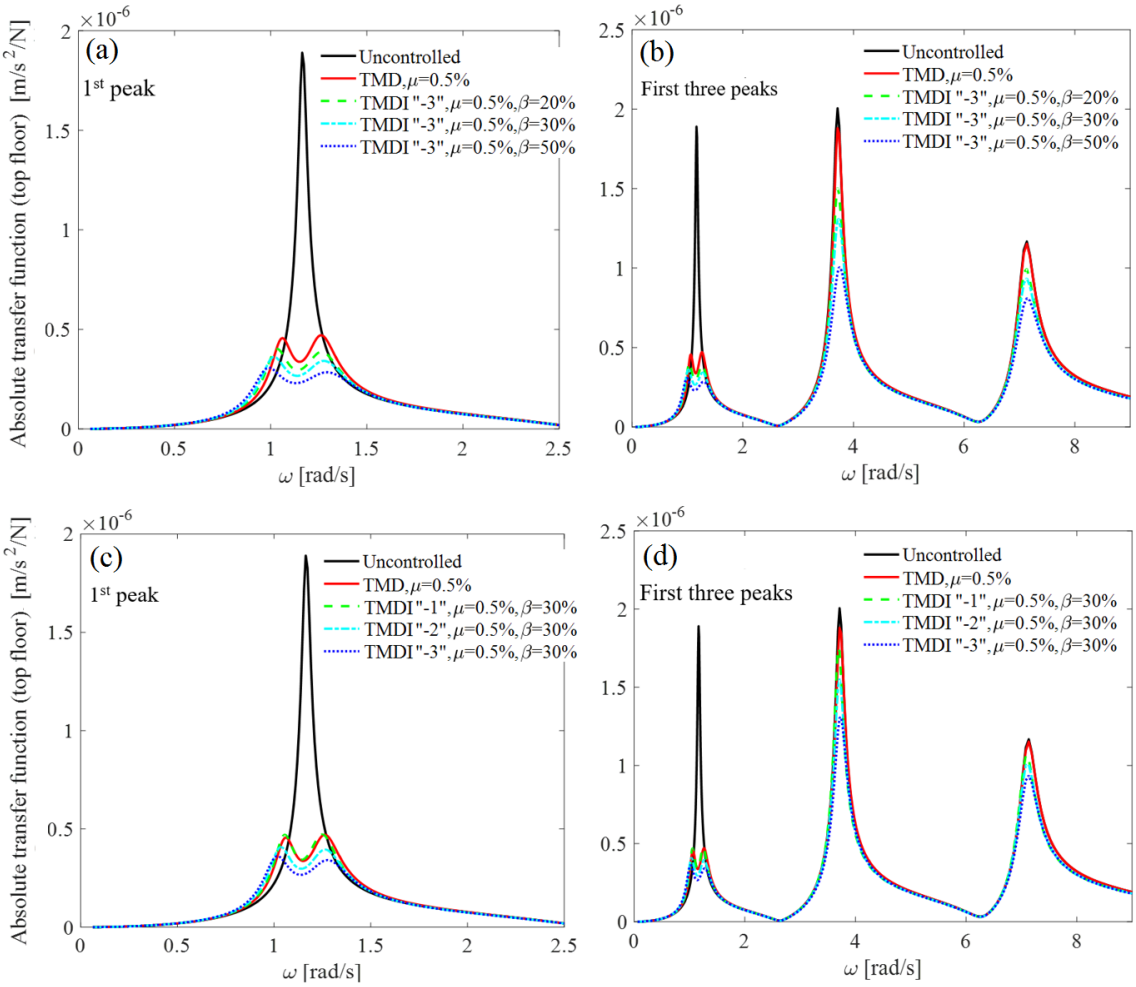

Figure 5. Amplitude of acceleration frequency response functions at the top floor of the case-study structure, $\omega^2|B(74,74)|$, with no motion control (uncontrolled), and controlled with TMD and TMDIs for fixed μ=0.5% and for different TMDI topologies and inertance ratios optimally designed for V_{ref}=30m/s.

4.3 Sensitivity of primary optimal design parameters to secondary parameters and to wind velocity

Turning the attention to the TMDI primary design parameters in $\mathbf{x_1}$, Fig. 6 plots iso-value curves of the optimal parameters υ_{opt} and ξ_{opt}, related to the TMDI stiffness and damping properties respectively, on the plane of the secondary design parameters in $\mathbf{x_2}$ (i.e., the μ-β TMDI *inertial design plane*) obtained by solving Eq.(21) for V_{ref}=30m/s and TMDI topologies "-1" to "-3". Note that the y-axis of the graphs in Fig.6 correspond to TMD optimal designs (β=0), while the x-axis corresponds to lightweight TMDIs with relatively low physical mass. It is seen in Fig.6(a) that υ_{opt} decreases with increasing inertance ratio for fixed secondary mass as well as with increasing mass ratio for fixed inertance for all considered TMDI topologies. Further, increasing the number of floors spanned by the inerter, results in faster changes of υ_{opt} with β, that is, iso-value υ_{opt} curves of the "-3" TMDI topology are steeper than of the "-2". Still, deviations of TMDI υ_{opt} values from those obtained for TMD cases are relatively small. Nevertheless, the variation of ξ_{opt} on the TMDI inertial design plane in Fig.6(b) is more significant. In particular, ξ_{opt} increases monotonically with increasing μ for fixed β. Further, it increases monotonically with β for fixed μ for all the considered TMDI topologies only for β>15%, while ξ_{opt} is more sensitive to differences in TMDI topology compared to υ_{opt}.

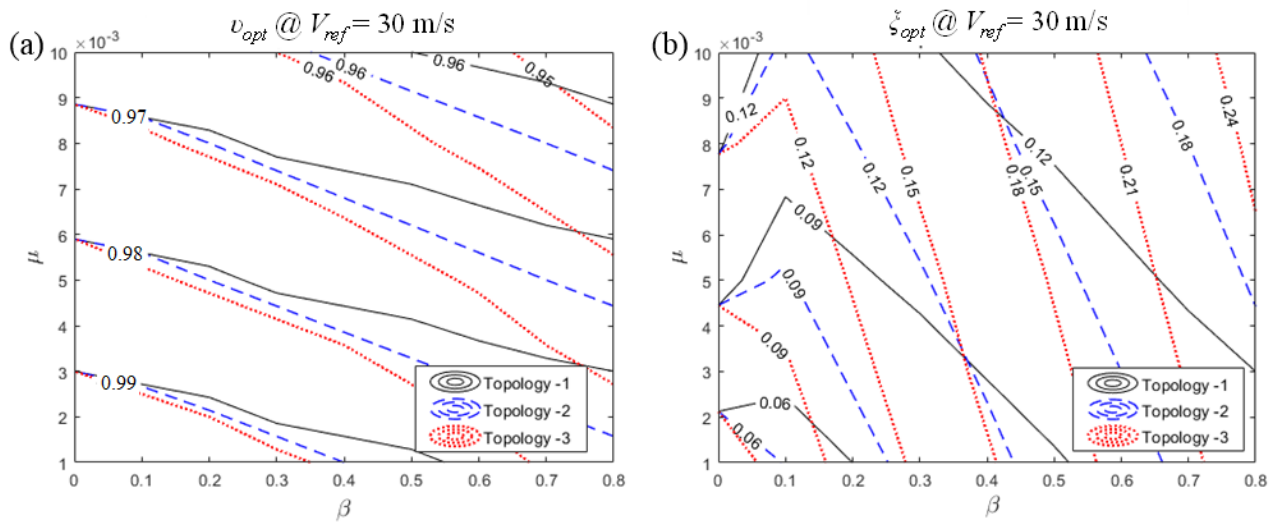

Figure 6. Optimal values of the primary design parameters in $\mathbf{x}_1$ on the secondary design parameters plane.

The sensitivity of the optimal design values in $\mathbf{x_1}$ is further quantified against changes to the reference wind velocity, V_{ref}, in Fig. 7, for the three considered TMDI topologies, one low inertance ratio value, β=0.1 and one very high inertance value, β=0.8, for fixed mass ratio μ=0.5%. Such changes to V_{ref} may be due to climate change effects predicted to increase V_{ref} at a given location in the foreseen future as discussed in [42]. It is important to note that changes to V_{ref} not only change the intensity of wind excitating forces, but also the

dominant excitation VS frequency through Eqs. (6) and (7). It is seen that optimal $\mathbf{x}_1$ values are at large insensitive and, therefore, robust to V_{ref} variations. In particular, ξ_{opt} remains practicality constant with V_{ref}, while υ_{opt} decreases only slightly with V_{ref} and only for the high β value considered.

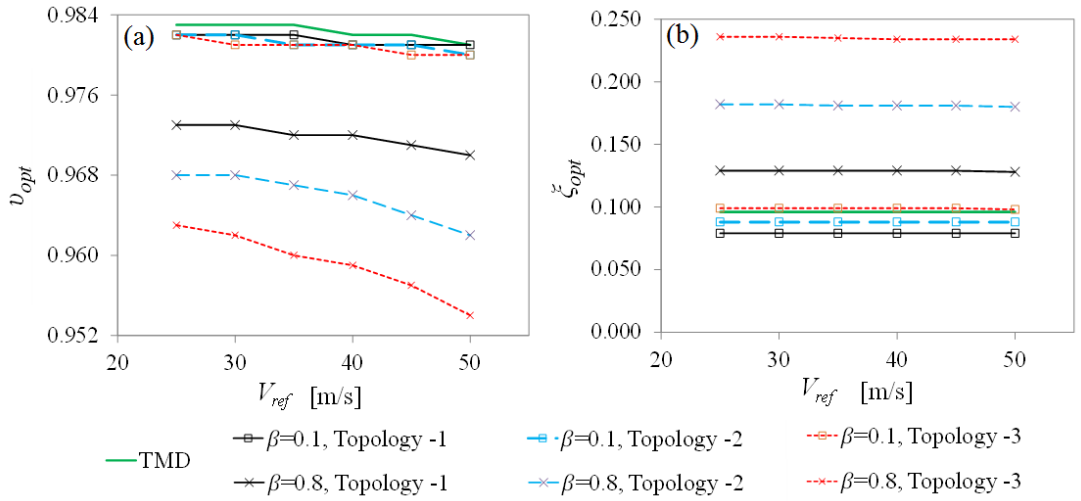

Figure 7. Sensitivity of the optimal values of the DVs to the variation of the wind speed. Case μ=0.5%

5 Performance-based assessment and design in optimally tuned TMDI-equipped structures

5.1 Peak top floor acceleration, secondary mass stroke, and inertance force

The efficiency of TMDIs designed/tuned through the optimization problem in Eq.(21) to contain VS induced vibrations causing occupants' discomfort in tall/slender structures can be quantified in a practically useful manner by evaluating the OF in Eq.(21), i.e., peak top floor acceleration of the case-study structure, for optimal parameters in $\mathbf{x}_1$ determined for various TMDI topologies and inertial properties in $\mathbf{x}_2$. To this aim, Fig. 8 plots three different families of iso-value curves of $\text{peak}\{\ddot{x}_{74}\}$ achieved by optimally tuned TMDIs in three different topologies on the β-μ plane. These curves are obtained by using optimal values for the TMDI primary design parameters, υ_{opt} and ξ_{opt}, reported in Fig.6 for V_{ref}=30m/s. It is seen that improved structural performance in terms of peak floor acceleration can be achieved by increasing the secondary TMDI mass for fixed inertance across the board. Further, improved structural performance is monotonically achieved with increasing inertance for the "-3" TMDI topology for fixed mass ratio as long as μ<0.6%. This is readily explained by examining the FRFs plotted in Fig. 5(b) whose peak values are reduced as inertance increases at all structural natural frequencies and not just the first/fundamental one and by noting that response acceleration are sensitive to high frequency dynamics. Interestingly, TMDs with μ>0.3% perform better than TMDIs in "-

1" and "-2" topologies with relatively low inertance ratios β<15%. However, as the inertance ratio increases above 15%, all TMDIs outperform TMDs for any fixed attached mass ratio providing improved performance with increasing inertance verifying trends reported in [25] for the case of non-optimal TMDIs. Importantly, it is deduced by comparing the slopes of the different families of the iso-value curves that the more floors the inerter spans, the faster is the rate of improved performance with increasing inertance. Consequently, better performance is achieved for sufficiently large fixed inertance ratio as the inerter spans more floors (see also FRFs in Fig. 5(d)).

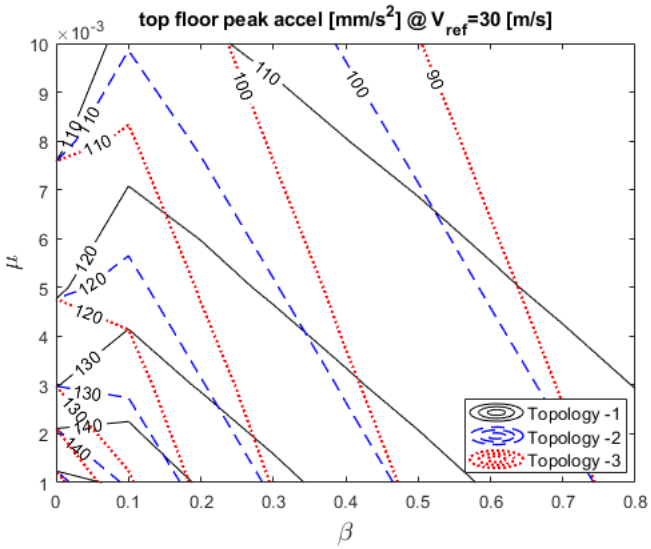

Figure 8. Peak top floor acceleration achieved with optimally designed TMDIs in different topologies and inertial properties: secondary mass ratio μ and inertance ratio β.

Apart from the improvement to host structural performance, an important response quantity of interest to the practical design of mass/inertial dampers is the so-called peak stroke of the secondary mass, that is the peak relative displacement of the TMD(I) mass with respect to the floor that the mass is attached to. This is because increased TMD(I) stroke demands require larger clearance in housing safely a TMDI within the host structure such that no local pounding/collision occurs. Further, the cost of energy dissipation devices/dampers increases with stroke. For the case-study structure, the peak stroke is computed by setting k=74 and l=75 (i.e., DOF corresponding to the x_{TMDI} displacement in Fig.3) in $\text{peak}\{x_{kl}\}$ expression in Eq.(17). Peak TMDI stroke values obtained for optimal TMDIs in three different topologies for the case-study structure for V_{ref}=30m/s are plotted in Fig. 9 as functions of TMDI inertial properties within the ranges $0.1\% \le \mu \le 0.55\%$ and $0 \le \beta \le 10\%$. Considerable stroke demand reduction is observed with increasing inertance for any fixed mass ration value as has been also the case for non-optimal TMDIs in [25]. For example, as illustrated in Fig.9, a ten-fold

reduction of the peak stroke (from 600mm to 60mm) is achieved by increasing the inertance from 0.5% to 9.5% for fixed mass ratio μ=0.2%. Interestingly, appreciable stroke reduction is achieved with increased mass ratio for only relatively small inertance ratios as the iso-value peak stroke curves in Fig.9 tend to become parallel to the y-axis with increasing β. Further, it is seen that stroke is insensitive to TMDI topology.

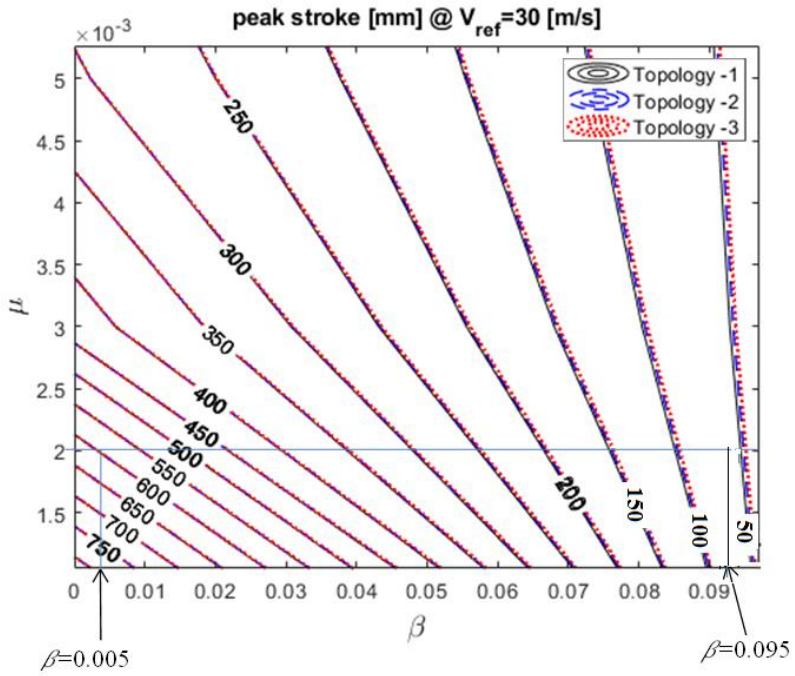

Figure 9. Peak stroke of optimally designed TMDI in the secondary design parameters plane

Having established that TMDI achieves better motion control with respect to TMD through increase of inertance and/or through considering TMDI topologies in which the inerter spans more floors, it is deemed useful to examine the peak inerter force in Eq.(9) developing for optimal TMDIs of different topologies as β increases. Figure 10 serves this purpose by plotting iso-value curves on the β-μ plane of peak inerter force developing in the case-study structure for different TMDI topologies under V_{ref}=30m/s. These curves are determined by setting k=74-p and l=75 in $\text{peak}\{\ddot{x}_{kl}\}$ expression in Eq.(17) in conjunction with Eq.(9). Trivially, inerter force is zero for β=0. Then, inerter force demands increase monotonically with inertance but at a gradually reduced rate. It is further observed that for β>10%, the inerter force increases for fixed inertance as the inerter spans more floors while variations to the inerter force among different TMDI topologies become more significant with decreasing attached mass. These observations verify that key to the efficacy of the TMDI for motion control is the inerter force. Indeed, larger inerter forces correlate well with more significant peak floor acceleration reductions as can be inferred by comparing iso-value curves in Figs. 8 and 10. Still, it is seen

that even for very large inertance ratios and for "-3" topology, the peak developing inerter force, at least for V_{ref}=30m/s, is not excessively large, as is the case for the use of TMDIs for seismic protection of buildings structures [43], and can be accommodated locally by the structure with some appropriate local detailing.

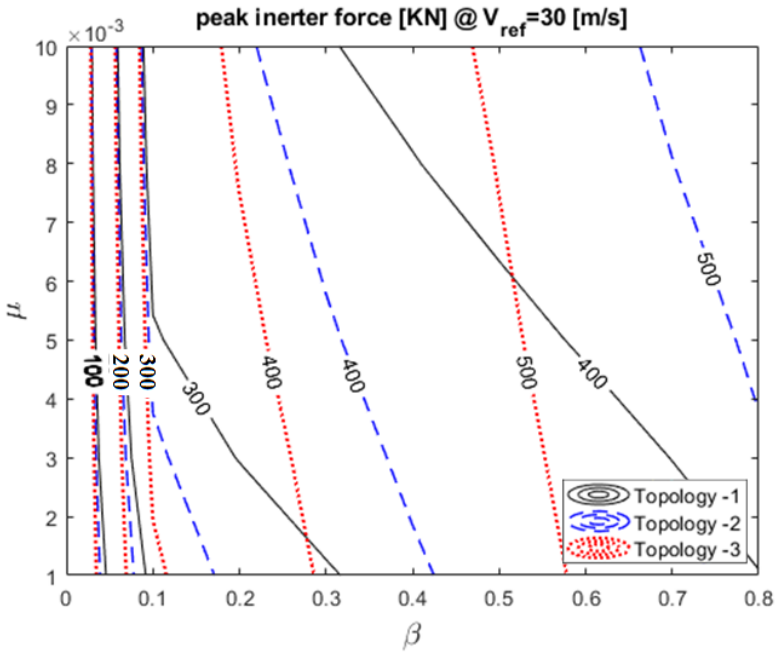

Figure 10. Peak inerter force of optimally designed TMDI in the secondary design parameters plane

5.2 Trading secondary mass to inertance

In the previous section, Fig.8 was used for comparative quantitative assessment of the potential of optimal TMDIs with different topologies and inertial properties to reduce floor accelerations in the case-study structure. Herein, the iso-value curves of Fig.8 are interpreted as TMDI design charts *from a performance-based design perspective* to demonstrate that mass ratio and, therefore weight, can be effectively traded for inertance for any desired pre-specified/target structural performance level in terms of peak floor acceleration related to occupants' comfort criteria [6,7]. To this aim, Fig. 11(a) plots the data of Fig. 8 pertaining to TMDI topology "-3" which was arbitrarily chosen for the sake of exemplification. Treating Fig.11(a) as a design chart, it is seen that any particular peak floor acceleration value can be achieved by TMDIs with different sets of inertial properties μ and β. Importantly, it is seen that in most cases the iso-value curves have negative slope on the β-μ plane. Therefore, optimized TMDIs with reduced secondary mass can achieve the same performance through increased inertance. This establishes a direct mass reduction/substitution effect endowed by the inerter

to the TMDI and leading to overall more lightweight inertial dampers: *a practically important advantage in designing new slender minimal-weight tall buildings*. To further illustrate this point, Fig. 11(b) plots iso-value curves for different TMDI topologies for peak top floor acceleration equal to the occupants comfort threshold, 102.9mm/s^2, applicable to the case-study structure assuming residential occupancy according to guidelines effective in Italy [44] (see also [13]). Evidently, the more floors the inerter spans the more significant the weight reduction effect becomes with increasing inertance as the iso-value curves become steeper going from "-1" to "-3" topologies, and, at the same time, inertance demands are reduced for fixed mass ratio in achieving the targeted performance.

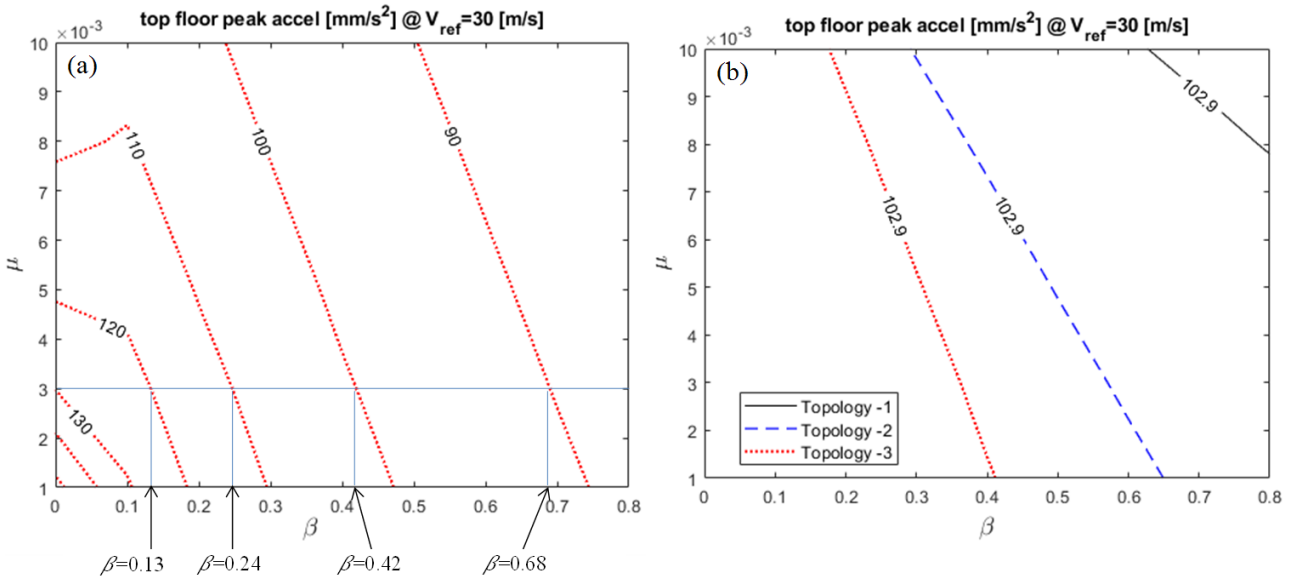

Figure 11. Performance-based design charts of TMDI for the case-study structure (a) Topology "-3"; (b) Various topologies for case-study structure occupants' comfort threshold 102.9mm/s^2.

Further to the case of new structures, the incorporation of an inerter, alongside retuning to achieve optimal parameters υ_{opt} and ξ_{opt}, is also applicable as a *retrofitting strategy in existing TMD-equipped tall buildings* to enhance their performance against wind excitation required by change of use/occupancy (e.g., from residential to office building) or by increasing V_{ref} (e.g., due to changes to wind exposure [34] or due to climate change effects [42]). Along these lines, an illustrative example is shown in Fig. 11(a) which assumes the scenario that the case-study building has a TMD with μ=0.3% already installed achieving 130mm/s^2 peak top floor acceleration under V_{ref} = 30m/s. By incorporating an inerter with β= 13%, 24%, 42%, or 68% at TMDI topology "-3", performance increases through reduction of peak top floor acceleration by 7.7%, 15.4%, 23.1%, or 30.8% respectively upon optimal retuning.

6 Performance assessment of non-optimally designed TMDI structure

6.1 Robustness to detuning due to changes of benchmark structure properties

Numerical data reported in previous two sections concern optimally designed TMDIs for a pre-specified reference wind velocity assuming perfectly known structural properties of the case-study structure. Nevertheless, as discussed in the introduction, TMD(I)s may be "detuned" either over time due to changes to the properties of the host building structure, or due to inaccurate knowledge of structural properties. In this respect, it is herein deemed useful to gauge the robustness of TMDIs of different topologies and inertial properties to mitigate peak floor acceleration under wind excitation in case the actual case-study structure has different properties from those assumed in optimal TMDI tuning. To this aim, the mass and damping matrices of the case-study structure defined in section 2.1 are perturbed by uniformly scaling them down by 10% and 20% of their original values, respectively. Mass perturbation consideration is related to uncertainty in mass density of materials as well as its occupancy and live loads during its service life, while damping perturbation consideration is motivated by large uncertainty in estimating inherent damping of tall buildings influenced, phenomenologically, by several parameters as discussed in [33] and references therein.

Figure 12 plots peak top floor acceleration versus inertance ratio for the case-study structure with perturbed mass and damping properties, respectively, and equipped with TMD(I)s optimally tuned to the original structure. In all cases, V_{ref}=30m/s for the incident wind is assumed and TMDIs with μ=0.2% and 0.5%, topologies "-1" and "-3" and inertance ratios β ranging from 0% (TMD) to 70% are considered. Further, to facilitate a comparison, the obtained accelerations are normalized by peak top floor acceleration of the original structure with optimal TMD(I)s. In this setting, the closer the ordinates of the graphs in Figs. 12(a) and 12(b) to unity is, the more robust the TMD(I) is to mass and damping property perturbations, respectively. In all the cases considered, it is seen that the TMDI is less robust than TMD for inertance ratios smaller than a relatively low critical value which depends on TMDI topology and mass ratio. These critical inertance ratios are reported in Table 2. It is found that the more floors are spanned by the inerter and/or the smaller the mass ratio, the lower the critical inertance ratios above which the TMDI becomes more robust than the TMD is. Then, as the inertance increases above the critical inertance ratios of Table 2, the TMDI becomes more robust at a rate that, again, depends on TMDI topology and mass ratio: the more floors are spanned by the inerter and/or the smaller

the mass ratio the faster increases the level of robustness with increasing inertance. In fact, the relatively lightweight TMDIs (μ=0.2%) with topologies "-2" and "-3" achieve higher robustness level than the "heavy" TMD (μ=0.5%) for inertance ratios lower than 25% and 20%, respectively, for both considered mass and damping perturbations. As a general comment, one concludes through inerters spanning more floors and through sufficiently large inertance the TMDI outperforms TMDs in terms of robustness to structural properties perturbation.

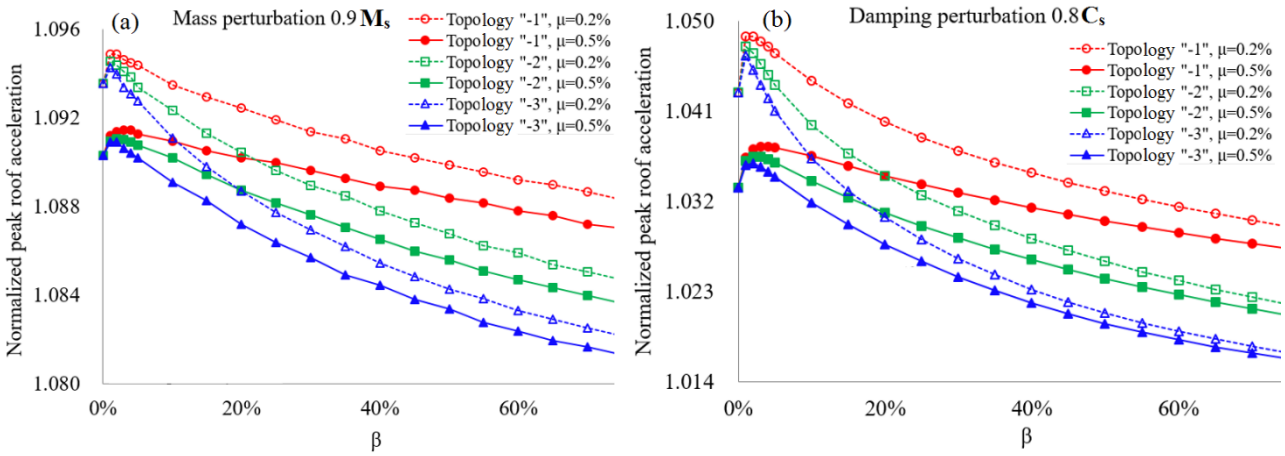

Figure 12. Robustness of optimally tuned TMDI to mass and damping properties perturbations of the case-study primary structure for V_{ref}= 30m/s.

Table 2. Critical inertance values (%) above which the TMDI is more robust from the TMD

	Topology	μ=0.2%	μ=0.5%
Mass perturbation $0.9\mathbf{M}_s$	-1	10.0%	20.0%
	-2	4.5%	9.5%
	-3	2.7%	4.8%
Damping perturbation $0.8\mathbf{C}_s$	-1	14.0%	27.5%
	-2	5.5%	11.0%
	-3	3.5%	6.5%

6.2 Performance for increased reference wind velocity, V_{ref}

In Fig.7 (section 4.3), it was found that optimal TMDI tuning parameters are quite robust to increasing reference wind velocity resulting in increasing amplitude and dominant frequency of the wind forcing field. This observation motivates investigating the potential of incorporating an inerter device to retrofit an existing structure equipped with a TMD optimally tuned to a particular V_{ref}, such that improved performance is achieved for a significantly higher V_{ref}. In doing so, it is assumed that no retuning takes place to the TMD which results in a non-optimal TMDI as opposed to optimal TMDIs for retrofitting of existing TMD-equipped structures

discussed in section 5.2 (Fig. 11(a)). In this regard, the herein considered retrofitting scenario for existing TMD-equipped structures involves only adding an inerter, with no replacement/adjustment of any other TMD(I) device components. To this end, this is a quite appealing retrofitting scenario from a practical viewpoint due to its simplicity as well as in view of inerter devices with varying inertance through gearing (see e.g., [31]).

Figure 13 plots peak top floor acceleration for the case-study building equipped with an optimally designed TMD at V_{ref} = 30m/s with μ=0.5% subjected to wind force field with V_{ref} = 45m/s (i.e., 50% above the design one) and provided with an inerter with varying inertance (without any variation of other parameters) and for three TMDI topologies. Reported top floor acceleration is normalized to the peak top floor acceleration for the TMD equipped structure at the increased V_{ref} = 45m/s. Therefore, ordinates below unity in Fig. 13 signify improved TMDI performance compared to TMD for V_{ref} = 45m/s. Similar to Fig. 12, it is seen that there is a critical inertance value, different for each TMDI topology, below which the TMD performs better than the TMDI, ranging from β=3.1%, for "-3" topology, to β=8.5%, for "-1" topology. Incorporating an inerter with larger inertance from this critical value will result in an increasingly better performance compared to the original TMD of the existing structure. Therefore, the proposed retrofitting strategy is effective as long as sufficient inertance is considered together with an appropriate TMDI topology.

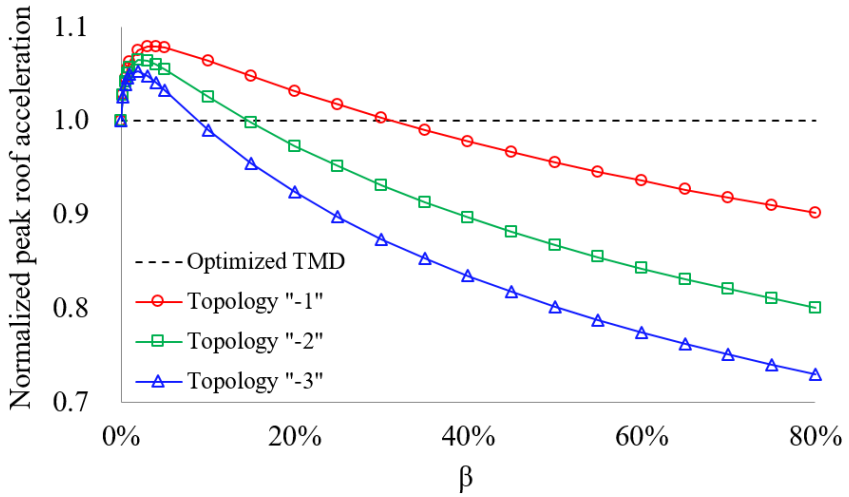

Figure 13. Comparative performance of non-optimal TMDI under V_{ref}=45m/s for retroffiting the case-study structure equipped with a TMD with μ=0.5% optimally tuned for V_{ref}=30m/s.

7. Energy harvesting potential from TMDIs with varying inertance and electrical damping properties

7.1 Proposed energy harvesting enabled TMDI configurations in wind-excited tall buildings

Having established the benefits of the TMDI vis-à-vis the TMD for suppressing floor accelerations in wind-excited tall buildings, this section contributes a further investigation exploring the potential of TMDI for harvesting usable electric energy from VS-induced oscillations in tall buildings. To this aim, a standard linear translational electromagnetic motor (EM) coupled with energy harvesting (EH) circuitry is added to the TMDI configuration of Fig.3 in parallel to the stiffness and damping elements as shown in Fig.14.

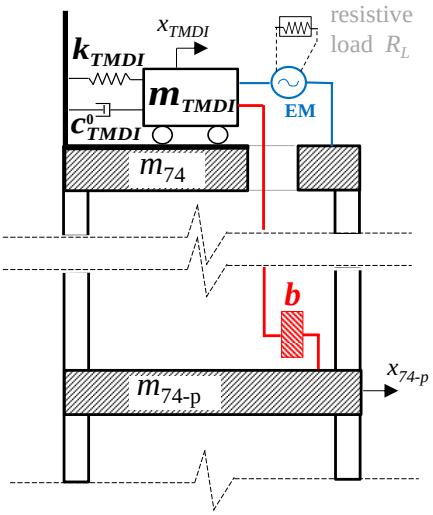

Figure 14. Proposed energy harvesting enabled TMDI for energy generation in wind-excited tall buildings

Compared to typical TMD-based energy harvesters previously considered in the literature for electric generation in oscillating tall buildings under wind excitation [17,18], the herein proposed energy harvesting-enabled TMDI (EH-TMDI) differs by the inclusion of the inerter device. The latter acts as an amplifier of the inertial/mass property of the motion control device which is found to be the key property in leveraging the trade-off between vibration suppression and energy harvesting potential in conventional regenerative TMDs scavenging energy from harmonic/narrow band excitations [21]. In this regard, note that the inerter functionality in the EH-TMDI is significantly different from inerter-based mechanisms and elements used as rotational motion amplifiers in various energy harvesting vibration controllers utilizing rack-and-pinion (e.g. [19]) or ball-screw mechanisms (e.g. [45-48]), similar to those used in flywheel-based inerters [26]. Further, the EH-TMDI in Fig. 14 differs from the configuration in [30] in that the second terminal of the inerter connects

to a floor within the tall building rather than being fixed to the ground which is mostly relevant for base isolated structures discussed in [49].

For the purposes of this work, an EM comprising a moving magnet within a coil is assumed with resistance R_c and inductance taken as negligible for the frequencies of interest in the application at hand [19,21]. Moreover, the EH circuit is assumed to be purely resistive with resistance R_L. Whilst this modelling assumption does not account for potential nonlinear behavior of actual EH circuits, it is deemed sufficient for the comparative quantification of the available energy for harvesting as the properties of EH-TMDI are let to vary [17,21]. Under the above assumptions, the electromechanical damping coefficient of the EM coupled with the EH circuit is given as [18,21]

$$c_{EM} = \frac{J^2}{(R_C + R_L)}, \tag{22}$$

where J is the magnetic field the EM with constant flux density, and the resisting damping force contributed by the EM element to the case-study structure in Fig.14 reads as

$$F_{EM} = c_{EM}(\dot{x}_{TMDI} - \dot{x}_{74}). \tag{23}$$

In this context, the damping matrix **C** of the EH-TMDI equipped surrogate model of the case-study structure is found by setting

$$c_{TMDI} = c_{TMDI}^0 + c_{EM} \tag{24}$$

In this regime, the maximum available energy for harvesting in all the ensuing numerical work is quantified as

$$EHpot = c_{EM}\left(\text{peak}\left\{\dot{x}_{75,74}\right\}\right)^2 \tag{25}$$

where the peak relative velocity between the terminals of the EH are evaluated as shown in Eq. (17) by setting k=75 and l=74. Clearly, the available energy for harvesting increases either by increasing the relative velocity of the secondary mass with respect to the top floor or by increasing the electromechanical damping coefficient in Eq.(22). Both the above effects are studied numerically in the following section for TMDIs tuned for minimizing peak top floor acceleration as safeguarding occupants comfort is expected to always be the priority in tall building design as opposed to energy harvesting potential maximization.

7.2 Quantification of concurrent vibration suppression performance and energy harvesting potential

From the structural dynamics viewpoint, the EM in Fig.14 can be seen as a damping device whose damping coefficient in Eq.(22) can vary in a passive-adaptive mode by changes to the EH circuit properties as discussed in [21,45]. In fact, such changes are frequently considered to leverage the trade-off between vibration suppression and EH through influencing the damping property in TMD-based energy harvesters [21]. This consideration is relevant to practical applications in which it may be desired to increase electric power generation during periods of time when vibration suppression requirements can be relaxed. In this respect, it may be applicable to tall office buildings: during off-hours minimal occupancy suggests that through varying the damping coefficient of the EM, larger amount of energy can be harvested since the serviceability limit state in terms of occupants' comfort (i.e., peak floor acceleration threshold) can be alleviated. Moreover, in the proposed EH-TMDI of Fig.14, it is further of interest to investigate whether the same trade-off may be leveraged through changes to the inertance achieved through gearing as previously discussed since this has been proved to be the case for the EH-TMDI with grounded inerter in [30].

To examine the above considerations, Fig.15 provides numerical data pertaining to TMDI-equipped case-study structure optimally designed for μ=0.5%, V_{ref}=30 m/s, topology "-1", and three different inertance values in which the damping property c_{EM} is let to vary. Specifically, Fig.15(a) plots the square of the peak relative velocity of the TMDI with respect to the top floor, Fig.15(b) plots the maximum available energy for harvesting in Eq.(25), and Fig.15(a) plots the peak top floor acceleration. All quantities are plotted against c_{EM} and are normalized (i.e., "pinned") to the values attained by the TMDI with β=20% optimally designed to minimize the peak top floor acceleration. Further, the x-axis is normalized to the same optimal design assuming that c_{EM}=1 for $c_{TMDI}^{Opt} = c_{TMDI}^{0} + c_{EM}$ and $c_{TMDI}^{0} = c_{EM}$. In this context, the only optimally tuned TMDIs are those for which c_{EM}=1, while all other cases are non-optimal as c_{EM} varies while c_{TMDI}^{0} is kept constant to the optimal value of $c_{TMDI}^{0} = c_{TMDI}^{Opt}/2$. As expected, performance in terms of peak top floor acceleration decreases as c_{EM} deviates from the optimal value in Fig. 15(c), however, by increasing c_{EM} to values above the optimal $c_{EM} = c_{TMDI}^{Opt}/2$ peak available energy for harvesting *EHpot* increases at a saturating rate up to 50% more than *EHpot* for optimal c_{EM} for all fixed inertance values. Interestingly, this is achieved even though relative TMDI velocity reduces with increasing c_{EM}. For c_{EM} values of about twice the optimal c_{EM}, *EHpot* reaches a plateau

and, therefore, no gains are achieved by increasing its value further. Further from the gains of increasing the EM damping property to the available energy for harvesting, data in Fig.15 evidence that gains to *EHpot* are also achieved by reducing the inertance ratio at the expense of deteriorating floor acceleration performance. Therefore, judicial variations to the inertance and/or damping TMDI properties enable enhanced EH performance in tall wind excited buildings in times of reduced occupancy during which users' comfort requirements can be less stringent.

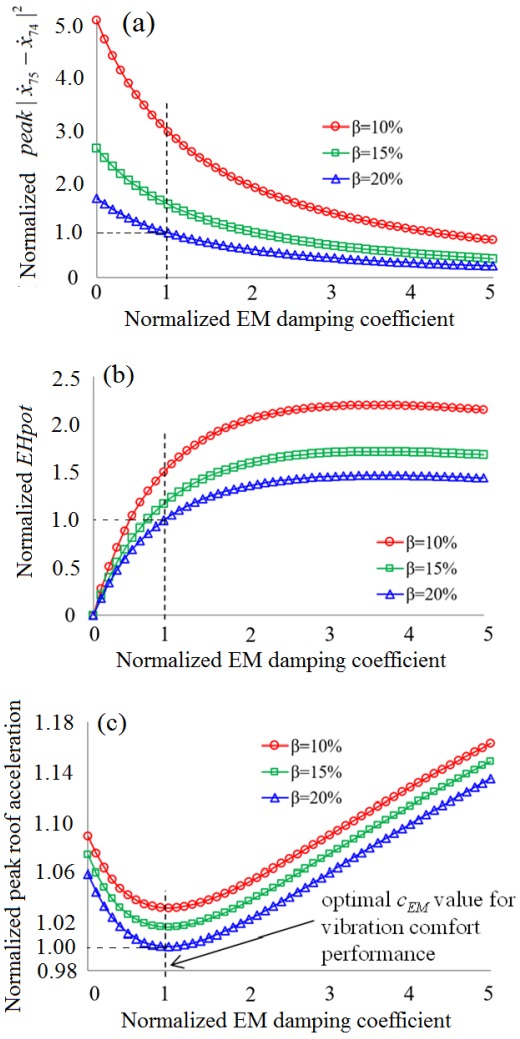

Figure 15. EH potential and performances of the EH-TMDI. μ=0.5%, V_{ref}=30m/s. Topology: -1, (a) peak relative velocity, (b) EH potential, (c) peak acceleration at top floor

To further investigate the effect of the EH-TMDI topology on the available energy for harvesting, *EHpot*, Fig. 16 plots similar data to Fig.15 but for fixed inertance ratio β=15% and three different topologies. In this case, all quantities plotted are normalized to values corresponding to optimal EH-TMDI minimizing peak top floor acceleration for "-1" topology. As expected, peak top floor acceleration reduces as the inerter

spans more floors. Remarkably though, relative TMDI velocity increases as the inerter spans more floor making, consequently, more energy available for harvesting. In this regard, considering EH-TMDI topologies in which the inerter spans more floors is beneficial for improved occupants' comfort as well as for harvesting kinetic energy in wind-excited tall buildings.

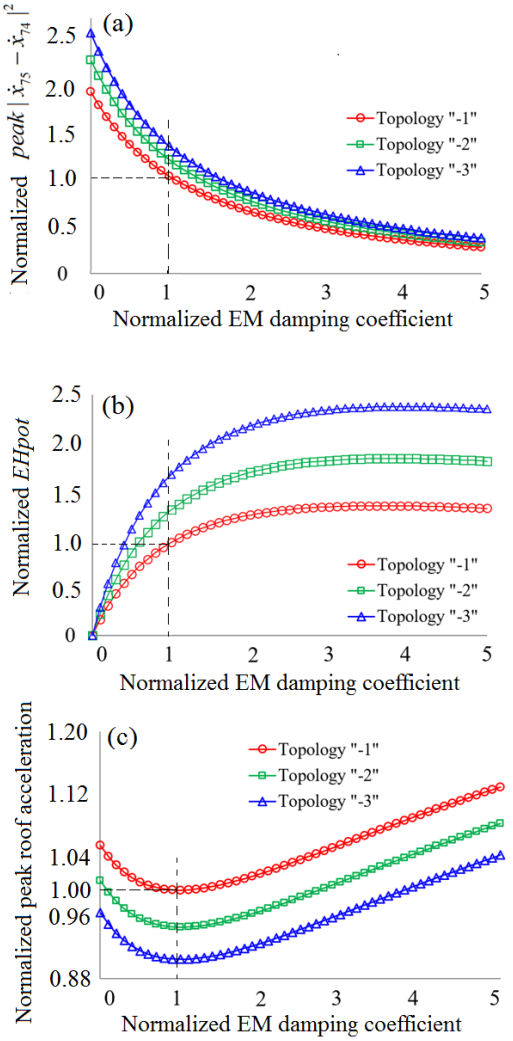

Figure 16. EH potential and performances of the EH-TMDI. μ=0.5%, V_{ref}=30m/s β=0.15. (a) peak relative velocity, (b) EH potential, (c) peak acceleration at top floor

8. Concluding remarks

The efficacy of the tuned mass damper inerter (TMDI) to achieve occupants' comfort performance and to harvest kinetic energy in wind-excited slender tall buildings susceptible to VS effects has been numerically established. Attention has been focused on exploring the influence and potential benefits of TMDIs with different inertial properties (i.e., secondary mass/weight and inertance) configured in different topologies

defined by the number of floors spanned by the inerter device to connect the secondary mass to the building structure. To this aim, a novel optimal TMDI design problem has been formulated to determine TMDI damping and stiffness properties such that the critical to buildings occupants' comfort floor acceleration in the across wind direction is minimized for pre-specified TMDI inertial properties and topology. Optimally designed TMDIs for a wide range of inertial properties and three different topologies have been obtained through numerical solution of the underlying optimization problem for a benchmark 305.9m tall building with more than 6 height-to-width ratio subjected to experimentally calibrated spatially-correlated across-wind force field accounting for VS effects in tall buildings with rectangular footprint. Computational work has been expedited by considering a surrogate low-order planar dynamical model of the benchmark building capturing faithfully structural dynamic behaviour along the critical wind direction as well as by performing frequency domain structural analysis.

High level of convexity in solving the optimization problem for all cases considered has been noted as well as robustness to TMDI optimal design parameters to varying reference wind velocity. Additionally, peak top floor acceleration FRFs for optimal TMDI-equipped structures demonstrated that TMDIs with fixed secondary mass/weight reduce FRF coordinates for all modes of vibration as opposed to solely mitigating the first/fundamental one in the case of the TMD. This wide-band mode-dampening effect was shown to be more significant as the inertance coefficient is increasing and/or as the number of floors spanned by the inerter increases. More importantly, innovative performance-based design graphs on the TMDI inertial (mass-inertance) plane have been furnished demonstrating that any fixed structural performance level in terms of occupants' comfort (i.e., peak top floor acceleration) may be achieved through replacing secondary mass by inertance as long as sufficiently large inertance, above a relatively low critical value, are considered. Further, the same graphs demonstrate that the more floors the inerter spans, the more significant mass reductions are achieved for same inertance. In this respect, it is concluded that more lightweight TMDIs for fixed performance are achieved through inerters spanning more floors and/or through increased inertance within an optimal TMDI design setting. Meanwhile, it was further shown that the stroke of the secondary TMDI mass is considerably reduced with increasing inertance, while peak inerter forces exerted to the host structure were shown to be of reasonable magnitude in all cases considered. To this end, the applicability of the reported performance-based design graphs to design new TMDI-equipped buildings as well as to retrofit existing TMD-equipped tall

buildings has been established. The latter case involves adding inerters spanning one or more floors to already installed TMDs with no changes to secondary mass to address increased requirements for occupants comfort and/or climate change effects expected to increase design reference wind velocity.

Robustness of optimally designed TMDIs to changes to the building structural properties, namely to total mass and inherent damping attributes, as well as to increased wind velocity, either due to increased wind exposure of the building and/or to climate change effects, was also explored. It was found that optimally tuned TMDIs become more robust than TMDs for same secondary mass as long as inertance above a certain limiting value is provided. This value depends on the secondary mass and on the number of floors spanned by the inerter: the lower the secondary mass and/or the more floors are spanned by the inerter, the lower the critical inertance value is. With regards to the energy harvesting potential of TMDIs achieved through standard EMs with EH circuitry, it was found that more kinetic energy is made available for harvesting by increasing the TMDI damping property (readily achieved through changes to EH circuitry) and/or by reducing the inertance (readily achieved through gearing). Nevertheless, such changes deviate from optimal TMDI and, therefore, deteriorate floor acceleration performance. It was, therefore, argued that by relaxing occupants' comfort requirements (i.e., serviceability limit state thresholds for floor accelerations) in wind-excited tall buildings based on occupancy considerations (e.g., off-hours in an office building) renders possible an increase in energy generation to be used to power wireless sensors and actuators required used for climate control or health monitoring in modern structures. More importantly, it was also found that the more floors the inerter spans, the higher the available energy for harvesting becomes and, simultaneously, the more improved performance in terms of occupants' comfort is achieved.

Overall, the furnished numerical data suggest that the proposed optimal TMDI design formulation yields practically meaningful performance-based design charts for occupants' comfort, while sufficiently large inertance values and/or TMDI topologies in which the inerter spans more floors are beneficial for occupants' comfort in VS-induced vibrations in tall buildings, for reducing secondary mass stroke, and for increasing robustness to building structural properties and wind intensity. Increased energy can be harvested at the expense of occupants' comfort through judicial changes to damping and inertance properties, while the more floors the inerter spans the more improved floor acceleration performance is achieved and, concurrently, the more energy is made available for harvesting. Note, however, that the above conclusions are valid for ideal linear inerter

behaviour and for ignoring nonlinear behaviour of the EM and the EH circuitry. Further work is warranted to verify the above findings in case of non-ideal/nonlinear inerters and for EH accounting for nonlinear electromechanical coupling effects. Moreover, the quantification of energy generation from wind on a yearly basis or in building lifetime requires treatment of mean wind velocity and direction as random variables and is left for future work.

Acknowledgements

This work has been funded by EPSRC in UK, under grant EP/M017621/1. The first two authors gratefully acknowledge this financial support.

References

[1] Taranath SB. Tall Building Design, Steel, Concrete, and Composite Systems. Boca Raton, FL: CRC Press; 2017.

[2] MASNYC - The Municipal art Society of New York. The Accidental Skyline 2017. Report MASNYC 2017. Available at https://www.mas.org/pdf/accidental-skyline-report-10-15-2017-web.pdf.

[3] Liang S, Liu S, Li QS, Zhang L, Gu M. Mathematical model of across-wind dynamic loads on rectangular tall buildings. J Wind Eng Ind Aerodyn 2002; 90:201-251.

[4] Tanaka H, Tamura Y, Ohtake K, Nakai M, Kim, YC. Experimental investigation of aerodynamic forces and wind pressures acting on tall buildings with various unconventional configurations. J Wind Eng Ind Aerodyn 2012;107-108: 179-191.

[5] Huang M. High-rise buildings under multi-hazard environment. Singapore: Springer Nature; 2017.

[6] Tamura Y, Kawana S, Nakamura O, Kanda J, Nakata S. Evaluation perception of wind-induced vibration in buildings. Proceedings of the Institution of Civil Engineers - Structures and Buildings 2006; 159(5):283-293.

[7] Kwok KCS, Hitchcock PA, Burton MD. Perception of vibration and occupant comfort in wind-excited tall buildings. J Wind Eng Ind Aerodyn 2009;7:368–380.

[8] Ierimonti L, Caracoglia L, Venanzi I, Materazzi AL. Investigation on life-cycle damage cost of wind-excited tall buildings considering directionality effects. J Wind Eng Ind Aerodyn 2017; 171:207-218.

[9] Caracoglia L. Unified Stochastic Dynamic and Damage Cost Model for the Structural Analysis of Tall Buildings in Thunderstorm-Like Winds. ASME J Risk Uncertainty Part B 2018; 4(4):04018043.

[10] Deng T, Fu J, Zheng Q, Wu J, Pi Y. Performance-Based Wind-Resistant Optimization Design for Tall Building Structures. J Struct Eng 2019;145:04019103.

[11] Bernardini E, Spence SMJ, Kwon D, Kareem A. Performance-Based Design of High-Rise Buildings for Occupant Comfort. J Struct Eng 2015; 141(10):04014244.

[12] Ciampoli M, Petrini F. Performance-Based Aeolian Risk assessment and reduction for tall buildings. Prob Eng Mech 2012; 28:75–84.

[13] Petrini F, Ciampoli M. Performance-based wind design of tall buildings. Struct Infrastruct Eng 2012; 8(10):954-966.

[14] Elias S, Matsagar V. Wind response control of tall buildings with a tuned mass damper. J Build Eng 2018; 15:51-60.

[15] Tse K, Kwok K, Tamura Y. Performance and Cost Evaluation of a Smart Tuned Mass Damper for Suppressing Wind-Induced Lateral-Torsional Motion of Tall Structures. J Struct Eng 2012: 138(4):514-525.

[16] Ierimonti L, Venanzi I, Caracoglia L. Life-cycle damage-based cost analysis of tall buildings equipped with tuned mass dampers. J Wind Eng Ind Aerodyn 2018; 176:54-64.

[17] Ni T, Zuo L, Kareem A. Assessment of Energy Potential and Vibration Mitigation of Regenerative Tuned Mass Dampers on Wind Excited Tall Buildings. 2011 ASME Design Engineering Technical Conferences; Washington DC, 2011, August 28–31.

[18] Shen W, Zhu S, Xu Y-L, Zhu H-P. Energy regenerative tuned mass dampers in high-rise buildings. Struct Control Hlth 2018; 25(1): e2072.

[19] Tang X, Zuo L. Simultaneous energy harvesting and vibration control of structures with tuned mass dampers. J Intell Material Syst Struct 2012; 23(18):2117–2127.

[20] Shen W, Zhu S, Xu Yl. An experimental study on self-powered vibration control and monitoring system using electromagnetic TMD and wireless sensors. Sens Actuator A-Phys 2012; 180:166- 176.

[21] Gonzalez-Buelga A, Clare LR, Cammarano A, Neild SA, Burrow SG, Inman DJ. An optimised tuned mass damper/harvester device. Struct Control Hlth 2014; 21(8):1154-1169.

[22] Gkoktsi K, Giaralis A. A multi-sensor sub-Nyquist power spectrum blind sampling approach for low-power wireless sensors in operational modal analysis applications. Mech Syst Signal Pr 2019; 116:879-899.

[23] Petrini F, Gkoumas K. Piezoelectric energy harvesting from vortex shedding and galloping induced vibrations inside HVAC ducts. Energ Buildings 2018; 158:371–383.

[24] Shen W, Zhu S, Zhu H. Unify energy harvesting and vibration control functions in randomly excited structures with electromagnetic devices. J Eng Mech 2019; 145(1): 04018115.

[25] Giaralis A, Petrini F. Wind-Induced Vibration Mitigation in Tall Buildings Using the Tuned Mass-Damper-Inerter. J Struct Eng 2017; 143(9):04017127.

[26] Smith MC. Synthesis of Mechanical Networks: The Inerter. IEEE Trans Automat Control 2002; 47(10): 1648-1662.

[27] Marian L, Giaralis A. Optimal design of inerter devices combined with TMDs for vibration control of buildings exposed to stochastic seismic excitations. Proc,.11th ICOSSAR Int. Conf. on Structural Safety and Reliability 2013; CRC Press, NY, 1025-1032.

[28] Marian L, Giaralis A. Optimal design of a novel tuned mass-damper–inerter (TMDI) passive vibration control configuration for stochastically support-excited structural systems. Prob Eng Mech 2014;38:156–164.

[29] Giaralis A, Taflanidis AA. Optimal tuned mass-damper-inerter (TMDI) design for seismically excited MDOF structures with model uncertainties based on reliability criteria. Struct Control Health Monitor 2018; 25(2):e208.

[30] Marian L, Giaralis A. The tuned mass-damper-inerter for harmonic vibrations suppression, attached mass reduction, and energy harvesting. Smart Struct Syst 2017; 19(6):665–678.

[31] Brzeski P, Lazarek M, Perlikowski P. Experimental study of the novel tuned mass damper with inerter which enables changes of inertance. J Sound Vib 2017; 404: 47-57.

[32] Spence SMJ, Gioffrè M. Large scale reliability-based design optimization of wind excited tall buildings. Prob Eng Mech 2012; 28:206-215.

[33] Spence SMJ, Kareem A. Tall buildings and damping: A concept-based data-driven model. J Struct Eng 2014; 140(5): 04014005.

[34] Simiu E, Scanlan RH. Wind effects on structures, Fundamentals and application to design. New York: John Wiley & Sons; 1993.

[35] ISO (2007) Bases for Design of Structures—Serviceability of Buildings and Walkways Against Vibration. ISO 10137, International Organization for Standardization, Geneva.

[36] Dai J, Xu Z-D, Gai P-P. Tuned mass-damper-inerter control of wind-induced vibration of flexible structures based on inerter location. Eng Struct 2019; 199:109585.

[37] Watanabe Y, Ikago K, Inoue N, Kida H, Nakaminami S, Tanaka H et al. Full-scale dynamic tests and analytical verification of a force-restricted tuned viscous mass damper. In: 15th World Conference on Earthquake Engineering. Lisbon, Portugal 2012

[38] Nakamura Y, Fukukita A, Tamura K, Yamazaki I, Matsuoka T, Hiramoto K, et al. Seismic response control using electromagnetic inertial mass dampers. Earthq Eng Struct Dyn 2014; 43:507–27.

[39] Roberts JB, Spanos PD. Random vibration and statistical linearization. New York: Dover Publications; 2003.

[40] Davenport AG. Note on the distribution of the largest value of a random function with application to gust loading. Proc Inst Civil Eng 1964; 28(2):187–196.

[41] Charles A, Dennis Jr JE. Analysis of Generalized Pattern Searches. SIAM Journal on Optimization 2003; 13(3):889–903.

[42] Steenbergen RDJM, Koster T, Geurts CPW. The effect of climate change and natural variability on wind loading values for buildings. Build Environ 2012; 55: 178- 186.

[43] Ruiz R, Taflanidis AA, Giaralis A, Lopez-Garcia D. Risk-informed optimization of the tuned mass-damper-inerter (TMDI) for the seismic protection of multi-storey building structures. Eng Struct 2018; 177:836-850.

[44] CNR - National Research Council of Italy (2010). Guide for the assessment of wind actions and effects on structures; Guidelines CNR-DT 207/2008. https://www.cnr.it/en/node/2642.

[45] Cassidy IL, Scruggs JT, Behrens S, Gavin HP. Design and experimental characterization of an electromagnetic transducer for large-scale vibratory energy harvesting applications. J Intell Material Syst Struct 2011; 22: 2009-2024.

[46] Hendijanizadeh M, Sharkh SM, Elliott SJ, Moshrefi-Torbati M. Output power and efficiency of electromagnetic energy harvesting systems with constrained range of motion. Smart Mat Struct 2013; 22(12): 125009.

[47] Asai T, Araki Y, Ikago K. Energy harvesting potential of tuned inertial mass electromagnetic transducers. Mech Sys Signal Pr 2017; 84: 569-672.

[48] Zhu H, Li Y, Shen W, Zhu S. Mechanical and energy-harvesting model for electromagnetic inertial mass dampers. Mech Sys Signal Pr 2019; 120: 203-220.

[49] De Angelis M, Giaralis A, Petrini F, Pietrosanti D. Optimal tuning and assessment of inertial dampers with grounded inerter for vibration control of seismically excited base-isolated systems, Eng Struct 2019; 196: 109250.